NASA/TM-97-206219

F-16XL Wing Pressure Distributions and Shock Fence Results from Mach 1.4 to Mach 2.0

Stephen F. Landers and John A. Saltzman
PRC, Incorporated
Edwards, California

Lisa J. Bjarke
NASA Dryden Flight Research Center
Edwards, California

National Aeronautics and
Space Administration

Dryden Flight Research Center
Edwards, California 93523-0273

October 1997

NOTICE

Use of trade names or names of manufacturers in this document does not constitute an official endorsement of such products or manufacturers, either expressed or implied, by the National Aeronautics and Space Administration.

Available from:

NASA Center for AeroSpace Information
800 Elkridge Landing Road
Linthicum Heights, MD 21090-2934
Price Code: A16

National Technical Information Service
5285 Port Royal Road
Springfield, VA 22161
Price Code: A16

ABSTRACT

Chordwise pressure distributions were obtained in-flight on the upper and lower surfaces of the F-16XL ship 2 aircraft wing between Mach 1.4 and Mach 2.0. This experiment was conducted to determine the location of shock waves which could compromise or invalidate a follow-on test of a large chord laminar flow control suction panel. On the upper surface, the canopy closure shock crossed an area which would be covered by a proposed laminar flow suction panel. At the laminar flow experiment design Mach number of 1.9, 91 percent of the suction panel area would be forward of the shock. At Mach 1.4, that value reduces to 65 percent. On the lower surface, a shock from the inlet diverter would impinge on the proposed suction panel leading edge. A chordwise plate mounted vertically to deflect shock waves, called a shock fence, was installed between the inlet diverter and the leading edge. This plate was effective in reducing the pressure gradients caused by the inlet shock system.

NOMENCLATURE

AMRAAM	Advanced Medium Range Air-to-Air Missile
BL	butt line, in.
c	local chord length, in.
C_p	pressure coefficient, $(p - p_0)/q$
DFRC	Dryden Flight Research Center, Edwards, California
ESP	electronic scanning pressure
FS	fuselage station, in.
HSCT	High Speed Civil Transport
ID	inner diameter
LE	leading edge
LNSI	Large Normal Shock Inlet
M	freestream Mach number
NACA	National Advisory Committee for Aeronautics
NSI	Normal Shock Inlet
p	local pressure, lb/ft^2
p_0	ambient pressure, lb/ft^2
PCM	pulse code modulation
q	dynamic pressure, lb/ft^2
SLFC	Supersonic Laminar Flow Control
x	longitudinal distance, positive aft, in.
x/c	nondimensional chord location
α	angle of attack, deg
α_i	indicated angle of attack, deg
β	angle of sideslip, deg

INTRODUCTION

High-speed aerodynamics has received renewed interest with increased attention being directed toward the High Speed Civil Transport (HSCT), or second-generation supersonic transport. Application of laminar flow technology has been proposed for use in the HSCT design. Previous studies projected that laminar flow control could result in a greater than 25-percent reduction in total aircraft drag subsonically,[1] making laminar flow an important area of research which could save significant quantities of fuel. With the exception of one experiment flown on the F-16XL ship 1 at NASA Dryden Flight Research Center (DFRC), Edwards, California,[2] no supersonic flight testing of laminar flow control using highly swept wings has been conducted.

NASA, Rockwell International, Seal Beach, California, The Boeing Company, Seattle, Washington, and McDonnell Douglas Aircraft, Long Beach, California, have teamed together to further investigate how laminar flow can be achieved during supersonic flight. The F-16XL aircraft at DFRC was selected as the research aircraft for the program. The F-16XL ship 2 was chosen as the test bed for the experiment because its general planform is similar to the proposed HSCT, and this airplane can achieve flight conditions near Mach 2, similar to the HSCT design point.

Previous flight tests were performed on the F-16XL ship 1 aircraft using a laminar flow control suction panel.[2] These flight tests showed laminar flow could be obtained on highly swept wings at supersonic speeds using suction. A large laminar flow control suction panel will be flight tested to high chord Reynolds numbers to expand the knowledge base and provide confidence in the use of laminar flow control on the HSCT. The new laminar flow test article will extend to 60 percent of the chord, compared to approximately 30 percent for the first test article, making it almost twice as large.

In support of the planned Supersonic Laminar Flow Control (SLFC) experiment on the F-16XL, pressure distributions were obtained in-flight on the upper and lower surface of the left wing. The main objectives of these tests were to determine the presence, strengths, and location of local shocks which could invalidate or compromise the SLFC experiment and to evaluate the effectiveness of the shock fence in blocking the inlet diverter shock. Computational studies performed in support of the design of the SLFC experiment showed the existence of a strong inlet diverter shock and a canopy closure shock.[3,4] The inlet diverter shock, which appears on the lower surface, crosses the leading edge (LE) and alters the pressure distributions, possibly enough to cause premature transition. On the upper surface, the canopy closure shock reduces the uncontaminated flow area on the suction panel and the chordwise extent available for laminar flow.

This paper describes the results of the pressure measurements obtained on the upper and lower surfaces of the F-16XL ship 2 left wing. Pressures were obtained using externally mounted tubing at speeds from Mach 1.4 to Mach 2.0, between altitudes of 45,000 and 50,000 ft, and at indicated angles of attack from 0° to 4°.

The contributions to this effort by Gaudy Bezos-O'Connor, Stan J. Miley, Paul M. Vijgen, and Jeffery K. Viken are gratefully acknowledged. This team coordinated and performed the wind tunnel testing of the F-16 model at NASA Langley Research Center, Hampton, Virginia. Note that use of trade names or names of manufacturers in this document does not constitute an official endorsement of such products or manufacturers, either expressed or implied, by the National Aeronautics and Space Administration.

AIRCRAFT DESCRIPTION

Figure 1 shows the F-16XL ship 2 aircraft. It is a two-seat supersonic prototype multirole fighter aircraft. Propulsion is provided by one General Electric (GE), Lynn, Massachusetts, F110-GE-129 increased-performance engine (IPE) rated at 29,000 lb of thrust. The engine inlet is the Large Normal Shock Inlet (LNSI) found on F110-GE-129-engined F-16 models[5], as compared to the smaller Normal Shock Inlet (NSI) found on aircraft which

have the lower mass flow Pratt & Whitney, East Hartford, Connecticut, engines. The LNSI provides 56 in^2 more capture area than the NSI inlet for a total of 774 in^2 at the throat and has slightly different geometric proportions. To avoid ingesting the fuselage boundary layer, the inlet is displaced from the fuselage by the inlet diverter (fig. 2(a)). A shock fence was installed underneath the wing in an attempt to block the disturbance from the inlet diverter from reaching the wing leading-edge (fig. 2(b)).

The weapons systems were removed from the aircraft, including the 20-mm gun in the left S-blend area; however, the trough for the gun remained open for the initial part of the flight experiment (fig. 3(a)). The gun trough was faired for subsequent flights (fig. 3(b)).

A passive glove was mounted on the right wing to investigate leading-edge momentum thickness Reynolds number dependencies for leading-edge laminar flow (fig. 2(a)). The glove was instrumented for measuring pressures, temperatures, boundary-layer transition, and glove structural strain.[6]

The F-16XL wing is a double-delta configuration with 0° dihedral. The leading-edge sweep is 70° from butt line (BL) 41.5 to 136.1, and the airfoil is a National Advisory Committee for Aeronautics 64A. Outboard of BL 136.1, the sweep is 50°, and the airfoil is a modified biconvex. Leading-edge flaps are provided for low-speed lift augmentation on the outboard wing section and have a range from 6° up to 36° down. Fuel is stored in two tanks per wing: forward and aft. The upper surface of the wing blends into the fuselage, the same as a standard F-16 aircraft. Elevons and ailerons are located across the entire trailing edge of the wing for pitch and roll control.

EXPERIMENT DESCRIPTION

External chordwise rows of 0.046-in. inner diameter (ID) pressure belts were bonded on both the upper and lower surfaces of the left wing and faired into the wing surface to obtain surface static pressures. Two chordwise rows were installed on the upper and lower surfaces (figs. 4(a) and 4(b)). Fairing the belts to the wing was accomplished using a fuel tank sealant to create a ramp flush to the top of the pressure belts with a width-to-height ratio of approximately 10 (fig. 4(c)).

On the upper surface, the inboard row was located between BL 43.5 and BL 51.6. This row consisted of 52 usable pressure lines; likewise, the upper surface outboard row was located between BL 90 and BL 95 and consisted of 31 usable pressure lines. To obtain a high resolution of pressure measurements along the wing chord for defining the shock locations, many orifices were desired. Because a large number of tubes would have extended too far spanwise, these orifices were staggered in four configurations serially and flown on separate flights. For example in configuration 1, pressures were obtained between 0.01 nondimensional chord length (x/c) and 0.15 x/c at the inboard upper belts and between 0.04 x/c and 0.15 x/c on the upper outboard belts (fig. 4(a)). Data were obtained for this configuration over several flights. Then, the configuration 1 orifices were plugged, and the configuration 2 orifices were drilled in locations aft of 0.15 x/c. The forward-to-aft configuration progression was used because these pressure measurements were made by transducers located in an aft wing panel. Data were obtained for flight conditions similar to those obtained with configuration 1 for configurations 2, 3, and 4 on subsequent flights. As a result, the chordwise pressure distribution was measured from 0.01 to 0.62 x/c inboard and 0.04 to 0.51 x/c outboard. Tables 1–6 list the orifice locations (with changes from the previous configuration shown in bold), and table 7 lists the time sequence associated with each flight.

Separating the upper inboard pressure belts into three groups allowed the shock angles to be estimated near the fuselage by using groups A and C (fig. 4(a)). Group B orifices for the pressure belts remained in the same location during the entire flight program to allow checking from flight to flight of the entire pressure distribution to ensure repeatability.

Two sets of belts were also installed on the lower surface of the wing (fig. 4(b)). Both sets contained 31 usable tubes. Inboard, the installation started at BL 51.4 and extended to BL 56, while outboard the belts covered BL 83.1

to BL 88.1. Under configuration 2, the outboard belts were replaced with a new set mounted further inboard between BL 59.5 and BL 64.5. The chordwise distance of interest was not as extensive for the lower surface as the upper; therefore, the configuration was not changed. See tables 1–6 for locations. Because of the importance of accurately locating the inlet diverter shock, a high resolution was used at the forward sections.

The internal diameter for the lines was 0.046 in. The longest lines (inboard upper surface) were nearly 300 in. long, and the shortest lines (lower outboard) were 80 in. long. Lag was not considered an issue because of the extended duration on conditions for the test points. Using previously reported techniques for computing lag,[7–8] the time delay at an altitude of 50,000 ft for 300 in. is approximately 1 sec. This lag was considered acceptable because the aircraft stayed on conditions for at least 10 sec at each test point.

Data were obtained on the lower surface with and without an inlet diverter shock fence (fig. 2(b)). The fence was an aluminum plate 10 in. high, 90 in. long, and 3/8 in. thick. This plate was mounted on the forward Advanced Medium Range Air-to-Air Missile (AMRAAM) station hard points at BL 46. The plate had a rounded leading edge swept 60° with respect to vertical. The 60° leading edge is subsonic up to Mach 2; thus, the fence did not generate a leading-edge shock. The fence was intended to reduce inlet diverter shock disturbance. Such disturbance could contaminate the wing leading edge for the SLFC experiment and cause premature transition on the upper surface.

INSTRUMENTATION

The pressure transducers used were 32 port electronic scanning pressure (ESP) modules with a differential pressure range of ± 5.0 lb/in^2. The sample rate was 12.5 samples/sec. Data acquisition was provided by a 10-bit pulse code modulation system (PCM). No leading-edge pressure data were available for the left wing from the pressure belts for two reasons. First, wrapping the belts around the sharp leading edge would cause difficulties because of natural resilience of the tube. Wrapping and adhering the tubes around the leading edge would cause crimping and warping. Second, the leading-edge radius would increase by almost a factor of two because of the thickness of the pressure belts. Previous results from the F-16XL ship 1 experiment and an F-8 experiment, where belts were wrapped around a sharp leading edge, showed that the distribution is greatly altered from the pressures sensed through a set of flush-mounted orifices.[9]

Reference pressure was measured by an absolute pressure transducer plumbed to a 25-in^3 reference tank located in the nose. The tank was vented to the atmosphere through two 0.25-in. ports on the upper portion of the aircraft nose. A 0.25-in. ID tube connected the tank to the ESP modules. Five seconds worth of ground zeros were taken before and after the flight, and these data were time-averaged for each orifice. This zero was then subtracted from each test point.

Static and total pressures were measured from a research noseboom mounted at the apex of the nose cone. The boom was also instrumented with vanes to measure angles of attack and sideslip. Total temperature was measured from a standard production aircraft probe mounted on the lower surface of the forebody.

EXPERIMENTAL TECHNIQUE

Test points between Mach 1.4 and Mach 2.0 were flown at altitudes of 45,000 and 50,000 ft. To accomplish the pressure survey of the aircraft, a slow, level acceleration (Mach number increased at 0.02/sec) was performed. Such a slow acceleration allowed approximately 4 sec of stabilized conditions within plus or minus Mach 0.04, which is sufficient for taking data. Following the acceleration, a series of pushovers to lower angles of attack and level turns at increased angles of attack was flown ranging from 0° to 4° indicated angle of attack (α_i) for each Mach number.

Data taken during the constant angle-of-attack or constant Mach number test points were time-averaged over a 1-sec interval (13 samples) to obtain the pressure coefficients for each test point. Then, the ground zeros were

subtracted from these readings. The same flight conditions of pressure altitude and Mach number were repeated on subsequent flights with different pressure belt configurations to obtain the overall pressure distribution of the two wing chords.

Fifteen flights were accomplished with the left wing instrumented with pressure belts. Of those, 11 were without the shock fence, and 4 were with the shock fence mounted. Table 7 lists the configuration changes on the aircraft.

RESULTS AND DISCUSSION

Both upper and lower surface pressure measurements were obtained on the baseline wing. The primary purpose of these measurements was to determine the location of shocks which could be detrimental to the planned SLFC experiment. Data quality, upper surface pressure distributions, and lower surface pressure distributions are described next.

Data Quality

Initial examination of the pressure data reveals irregular, random scattering from orifice to orifice of approximately 0.02 C_p (fig. 5). Further investigation into this irregularity suggests several possible explanations. Small, circular areas of the pressure belts were observed by the aft flight crew member to lift up or bubble from the surface approximately 0.50 in. during the flights as a result of localized debonding. The lifted sections could alter the local flow characteristics and, therefore, the pressure field. These areas were mapped out and referenced to known locations on the wing. The crew member's view only extended to approximately 0.25 *x/c* on the inboard row.

Figure 5 shows flight data at Mach 1.9, an altitude of 50,000 ft, and an angle of attack of 3.4°. The arrows point to areas where the upper surface belts were observed to be lifted up. Longer arrow length indicates a larger area lifted. Of all the bubbled up areas that were affected, the largest was estimated to be approximately 2 in. in diameter, and the lift up was approximately 0.75 in. Other areas were debonded in the same way, which can account for the overall irregular shape of the curves. These areas were confirmed to be debonded during postflight inspections, and when possible, such areas were reattached.

Figure 6 shows flows from an oil flow test conducted at the NASA Langley Research Center, Hampton, Virginia, Unitary Plan Supersonic Wind Tunnel on a 1/15 scale model of the F-16XL ship 2. Test conditions were Mach 1.9 and an angle of attack of 3.3°, corresponding to the trimmed flight condition at an altitude of 50,000 ft. The baseline wing is shown. Behind the canopy, the flow turns toward the fuselage approximately 10° and then encounters what is being called the *canopy closure shock* which turns the flow outboard. A roughness similar to the pressure belts in angled flow can cause variations of approximately 0.04 C_p,[10] which is observed in the pressure distributions (fig. 5).

Note that C_p variations caused by pressure belt debonding are relatively small compared to the C_p change caused by shock waves. This difference indicates that these data are adequate for determining locations of shock waves. In all cases, the location of a shock wave was defined as the pressure port where a consistent pressure increase starts.

Upper Surface Pressure Distributions

Pressure distributions were measured on the upper surface of the wing to determine the location and strength of the canopy closure shock. The location of this shock was needed to determine how much of the test section planned for the SLFC experiment would be affected.

Influence of Gun Trough Protrusion

Figure 7 shows pressure distributions from the upper surface of the left wing near the gun trough. The solid areas on the inset show where the data were taken from on the pressure belts. Data are shown from flights with and without the gun trough fairing (figs. 3(a) and 3(b)) for Mach 1.4. Shock waves are indicated in the data without the gun trough fairing by the large increase in pressure starting at x/c = 0.075 in figure 7(a) and at x/c = 0.080 in figure 7(b). Because the orifices were spaced 2 to 3 in. apart, the resolution for determining the shock location is approximately 0.005 x/c.

Connecting the locations where the pressure increases start permits the mapping of the straight lines at each Mach number which represents the shock wave. See inserts in figure 7. The point where the lines from various Mach numbers converge locates the source of the shock wave.

The shock wave at Mach 1.4 nearly disappears with the installation of the gun trough fairing (fig. 7). The pressure distribution becomes nearly flat until passing the region influenced by the fairing. At Mach 1.7, a shock wave is still generated with the gun trough fairing, but at approximately one-half the strength as without the fairing and slightly further aft (fig. 8). The gun trough will be covered by the passive fairing in the SLFC experiment and will not have any protrusions to generate shocks. Subsequent data shown here are with the gun trough fairing installed.

Influence of Mach Number

Figure 9 shows a composite plot of the pressure data from the four configurations for Mach 1.4, at an altitude of 50,000 ft, and an angle of attack of 3.2°. A rapid expansion occurs just behind the gun trough fairing, as shown by a sharp decrease in the pressure around x/c = 0.12. The probable cause of this expansion is either the aft section of the canopy which starts to curve toward the centerline or the expansion ramp generated by the back side of the gun trough fairing (fig. 3(a)).

A pressure increase is observed on the group A orifices starting at x/c = 0.30 (fig. 9(a)). Correlating these data with the group C pressures (fig. 9(b)) and the outboard pressure belt data (fig. 9(c)), which shows the shock also at x/c = 0.30, the shock wave is generated from the aft section of the canopy near the fuselage. The furthest forward location where the pressure increase is observed will subsequently be referred to as the canopy closure shock.

At Mach 1.7 and an angle of attack of 3.3°, the gun trough shock is still visible for the group A orifices on the inboard belt, but it is barely perceptible on the group C orifices (figs. 10(a) and 10(b)). The general trend of the distribution is a slightly favorable gradient (i.e. negative) until the canopy closure shock, approximately x/c = 0.37 for group A orifices. Aft of the shock wave the gradient is nearly neutral to slightly adverse. The canopy closure shock can be seen on the outboard pressure belt at x/c = 0.45 (fig. 10(c)).

Data from Mach 1.9, at an altitude of 50,000 ft, and an angle of attack of 3.4° show similar trends as those at lower Mach numbers (fig. 11). As expected, the gun trough shock is slightly aft of the locations found at Mach 1.4 and Mach 1.7. The location of the canopy closure shock has moved aft to x/c = 0.41 on the inboard belt pressure orifices (figs. 11(a) and 11(b)). The canopy closure shock does not appear in the pressure distribution on the outboard pressure belt and is assumed to be aft of the instrumented region of the chord (i.e. >51 percent) (fig. 11(c)).

From the Mach 2.0 data on groups A and C of the upper inboard pressure belts (fig. 12), the gun trough shock can still be seen at x/c = 0.11. Near x/c = 0.41 on group A (fig. 12(a)) and x/c = 0.43 on group C (fig. 12(b)), the canopy closure shock is visible. Outboard, the distribution is generally a linear, favorable gradient with some small local variations (fig. 12(c)). Again, no shocks can be seen on the outboard station.

Figure 13 shows the location and strength of the canopy closure shock for Mach numbers between 1.4 and 2.0. As expected, the canopy closure shock moves aft with increasing Mach number. The strength of the shock also decreases. On the outboard orifice row, the shock can be seen up to Mach 1.7. At higher Mach numbers, the shock is behind the last orifice. Figure 13 also shows data for the gun trough location and strength. Similar to the canopy closure shock, the gun trough shock moves aft and decreases in strength with increasing Mach number. However, the gun trough shock is not as strong as the canopy closure shock.

Figure 14 shows a graphical representation of where the shock waves generated from the canopy closure area traverse the proposed suction panel for the SLFC experiment. This position could shift slightly because of the installation effects created by the suction panel and passive fairing.

Influence of Angle of Attack

Angle of attack has only a small influence on the upper surface pressure distributions at Mach 1.9 over a range from 2.4° to 4.4° (fig. 15). The pressure coefficient levels change slightly, but overall the shape of the pressure distribution remains the same, including the canopy closure shock location, which is true for all Mach numbers on this aircraft. Normal acceleration ranged from 0.5 g at 2.4° to 1.5 g at 4.4° for these test points.

Lower Surface Pressure Distributions

Pressure distributions were also measured on the lower surface of the left wing. These measurements were taken to determine whether any shocks existed that could result in steep adverse pressure gradients near the wing leading edge. Steep adverse pressure gradients near the leading edge of the SLFC experiment could cause premature boundary-layer transition.[11]

Influence of Mach Number

A shock wave predicted by preliminary computational solutions[3] became evident in the flight data from the inboard pressure row (fig. 16). Data are shown for Mach 1.4, Mach 1.7, and Mach 1.9 at indicated angles of attack of 2.0° and at an altitude of 50,000 ft. These measurements correspond to true angles of attack of 3.2° at Mach 1.4, 3.3° at Mach 1.7 and 3.4° at Mach 1.9. As expected, the shock moves aft with increasing Mach number, from x/c = 0.03 at Mach 1.4 to x/c = 0.065 at Mach 1.9. The shock strength also increases with Mach number.

Shock Fence Results

Figure 17 shows data from an altitude of 50,000 ft, at Mach 1.4, and at an angle of attack of 3.2° for the lower surface inboard belt. Cases with and without the shock fence installed are shown. Near x/c = 0.03, a shock wave occurs for the case without the shock fence. This shock emanates from the inlet diverter. Note that with the shock fence in place, the shock at x/c = 0.03 is no longer present. It is interesting to note that the shock fence also decreases the pressure from the leading edge to approximately x/c = 0.08.

Figure 18 shows data taken from the inboard lower surface belt for Mach 1.7, at an altitude of 50,000 ft, and an angle of attack of 3.3°. The shock wave starts at x/c = 0.05 on the inboard row in the absence of the fence. With the fence, the shock is no longer evident in the distribution.

At Mach 1.9, an altitude of 50,000 ft, and an angle of attack of 3.4° (fig. 19(a)), the shock fence is still effective at blocking the inlet diverter shock. Without the shock fence, the shock is at x/c = 0.064 at the inboard station. With the fence, the distribution is much flatter along the chord. Two pressure increases appear on the distribution

with the fence which could possibly be shocks: one near $x/c = 0.02$ and the other at $x/c = 0.09$. The source of the forward shock is discussed in the Influence of Angle of Attack subsection. The pressure increase near $x/c = 0.09$ does not appear to be caused by the shock fence which extends to nearly $x/c = 0.25$. No data exist which can conclusively show the origin of the apparent shock wave. However, the inlet diverter shock wave may cross over the fence, possibly further aft on $x/c = 0.09$, because of the three-dimensional nature of the shock wave.

Figure 19(b) shows outboard pressure belt 2. This belt was positioned between the inboard and the original outboard row because a shock was never seen on the original outboard belt. The shock wave crossed the outboard belt 2 at $x/c = 0.048$ without the fence, which when correlated with the inboard belts produces a line which points directly to the inlet diverter (fig. 20). With the shock fence, the shock wave is no longer present (fig. 19(b)).

Without the fence at Mach 2.0, an altitude of 50,000 ft, and an angle of attack of 3.5°, the shock wave shifts further aft to $x/c = 0.075$ (fig. 21(a)). The fence eliminates this shock at the inboard location. At the original outboard pressure belt (fig. 21(b)), the diverter shock wave still does not appear regardless of the absence or presence of the fence because the sweep of the shock wave is insufficient for it to cross the outboard row.

Influence of Angle of Attack

Figure 22 shows the influence of angle of attack on the lower wing surface pressure distributions with and without the shock fence at Mach 1.9, an altitude of 50,000 ft, and at angles of attack between 1.4° and 5.4°. Without the fence (fig. 22(a)), the inlet diverter shock begins at $x/c = 0.065$, and the gradient weakens with decreasing angle of attack. The magnitude of the gradient at an angle of attack of 5.4° is more than double that at 1.4°. At low angles of attack (1.4° and 2.4°), another shock occurs near the leading edge at $x/c = 0.02$ and 0.03. This shock moves aft with decreasing angle of attack and is only observed on the most forward orifices at lower angles of attack. This shock is not observed at high angles of attack because the shock has moved forward of the pressure orifices. The probable point of origin for this shock is the inlet lip.

Figure 22(b) shows the influence of angle of attack on the lower surface pressure distributions with the shock fence installed. At all angles of attack tested, the pressure rise was reduced by a factor of two or more when the shock fence was installed. The shock noted near the leading edge for angles of attack of 1.4° and 2.4° is further aft and weakened with the shock fence installed. At an angle of attack of 3.4°, the leading-edge shock is visible with the shock fence installed. This finding reinforces the supposition that this shock is ahead of the orifices at high angles of attack without the shock fence.

Oil flow photographs taken during wind tunnel tests (fig. 23) show the shock waves near the inlet. In figure 23(a), the test conditions are Mach 1.7 and at an angle of attack of 3.3°. The shock is not swept aft far enough to cover the area that was measured on the actual aircraft. At Mach 1.9 and an angle of attack of 3.3°, however, the shock is visible on the forward section of the S-blend.

The flight results show that the inlet lip shock was sensitive to angle of attack, and its position and strength also varied with altitude (fig. 24). It is unlikely that altitude has a major affect on the pressure coefficient in these cases. However, the inlet airflow decreases with increasing altitude. Because the inlet lip shock appears to be the cause of the disturbance near the leading edge, its shape or sweep may change with inlet airflow.

Figure 24 shows the lower inboard surface pressure at several altitudes, Mach 1.9, and at angles of attack of 1.4°, 2.4°, and 3.4°. At an angle of attack of 1.4° (fig. 24(a)), the shock moves further aft with increasing altitude (or decreasing airflow). One case does not exactly follow the trend. At an altitude of 46,100 ft, the shock is in the same location as at 50,000 ft, but the Mach number is also slightly higher. At 2.4° (fig. 24(b)) the same general trend is seen although there is little change in shock location between altitudes of 44,400 and 49,600 ft at this angle of attack. Again, one case at 50,900 ft does not follow the trend, but the Mach number is slightly lower than the rest. For 3.4°, the shock is barely apparent in the majority of cases (fig. 24(c)). The two extreme altitude cases (49,400

and 38,600 ft) follow the trend of the inlet shock moving aft with increasing altitude (decreasing airflow), and the middle altitudes are quite similar. The 49,400-ft case shows little evidence of an inlet lip shock, but the Mach number is slightly lower. The position of the inlet lip shock is, therefore, sensitive to angle of attack, Mach number, and altitude (inlet airflow).

CONCLUDING REMARKS

Chordwise pressure distributions were obtained during flight tests on the upper and lower surface of the left wing of the F-16XL ship 2 aircraft. The experiment was conducted to determine the presence and locations of shock waves that could affect the Supersonic Laminar Flow Control (SLFC) experiment. From these data, the following remarks can be made:

On the upper surface at the design conditions of Mach 1.9 and at an altitude of 50,000 ft, 91 percent of the proposed glove area was forward of the canopy closure shock. At Mach 1.4, however, only 65 percent was forward of the shock wave. The canopy closure shock will limit the chordwise Reynolds number available for laminar flow on the SLFC experiment. Angle of attack had no affect on the position of the canopy closure shock.

On the lower surface, the inlet diverter shock was observed which could impinge on the leading edge at Mach numbers between 1.4 and 2.0. A chordwise shock fence appears to be effective in reducing the inlet diverter shock effects.

The inlet lip also generates a shock wave which impinges on the lower surface of the wing near the leading edge. The chordwise position of the inlet lip shock wave is sensitive to angle of attack, altitude (inlet airflow), and Mach number. A chordwise shock fence decreases the strength of the inlet shock and moves it aft.

Accuracy of the pressure measurements may have been limited by two factors: (1) lifting of the pressure belts in localized areas and (2) localized crossflow angles which were too severe for the accurate use of pressure belts. Neither factor was sufficient to interfere with the ability to distinguish the shock waves from the noise in the pressure measurements.

A shock generated by the gun trough was observed on the upper surface of the wing. This shock was greatly alleviated by a simple fairing. The gun trough will not cause a problem for the upcoming SLFC experiment because the passive fairing covers the area entirely.

Dryden Flight Research Center
National Aeronautics and Space Administration
Edwards, California, April 19, 1995

REFERENCES

[1] Reshotko, Eli, "Drag Reduction by Cooling in Hydrogen-Fueled Aircraft," *J. of Aircraft*, vol. 16, no. 9, Sept. 1979, pp. 584–590.

[2] Anderson, Bianca T., Bruce H. Rowan, and Stephen F. Landers, *F-16XL Supersonic Laminar Flow Control Glove Initial Flight Test Results*, NASA TM-104270, 1993. [This document contains information that is subject to ITAR restrictions.]

[3] Blom, G. A, CFD Investigation of Inlet/Diverter/Fence Effects, Unpublished F-16XL-2 SLFC Aerodynamics Working Group Coordination Memorandum BO-XL-A-012, Sept. 21, 1993.

[4] Blom, G., V. Tat, and P. Parikh, Effects of Viscosity and Canopy Windshield Shock on Suction Panel Pressure Distribution, Unpublished F-16XL-2 SLFC Experiment Team Coordination Memorandum BO-XL-135, Aug. 20, 1993.

[5] Scofield, Jan W., Sheryl R. Scott, and Edwin A. Thomas, *F-16XL Phase I Flying Qualities Evaluation—Final Report*, AFFTC TR-83-26, Sept. 1983. [Distribution limited to U.S. Government Agencies. Refer other requests to ASD/YP, Wright Patterson AFB, Ohio 45433.]

[6] Anderson, Bianca T. and Marta Bohn-Meyer, *Overview of Supersonic Laminar Control Research on the F-16XL Ships 1 and 2*, NASA TM-104257, Oct. 1992.

[7] Lamb, J. P., *The Influence of Geometry Parameters Upon Lag Error in Airborne Pressure Measuring Systems*, WADC TR 57-351, July 1957.

[8] Whitmore, Stephen A., F-16XL Suction Panel Tubing Frequency Response, Unpublished Internal NASA Dryden Memorandum, Undated.

[9] Montoya, Lawrence C. and David P. Lux, *Comparisons of Wing Pressure Distribution from Flight Tests of Flush and External Orifices for Mach Numbers from 0.50 to 0.97*, NASA TM X-56032, 1975.

[10] Czarnecki, K. R. and William J. Monta, *Pressure Distributions and Wave Drag Due To Two-Dimensional Fabrication-Type Surface Roughness on an Ogive Cylinder at Mach Numbers of 1.61 and 2.01*, NASA TN D-835, 1961.

[11] Neumann, F., "Cycle 1, Sloping Roof Top (SRT) Final Glove," Unpublished F-16XL-2 Team Coordination Memorandum, BO-XL-126, July 22, 1993.

Table 1. Orifice locations for pressure belt configuration 1. (Distance measured from leading edge.)

Upper surface						Lower surface					
Inboard[a]			Outboard[b]			Inboard[c]			Outboard[d]		
Orifice	x in.	x/c	Orifice	x in.	x/c	Orifice	x in.	x/c	Orifice	x in.	x/c
1	53.0	0.151	53	1.6	0.007	1	7.1	0.022	32	11.3	0.045
2	50.7	0.145	54	21.2	0.090	2	8.1	0.025	33	12.3	0.049
3	48.5	0.138	55	41.4	0.175	3	9.1	0.028	34	13.4	0.053
4	46.3	0.132	56	61.3	0.259	4	10.2	0.031	35	14.4	0.057
5	44.0	0.126	57	81.2	0.343	5	11.2	0.034	36	15.3	0.061
6	41.6	0.119	58	34.2	0.145	6	12.2	0.037	37	16.3	0.065
7	39.6	0.113	59	33.2	0.140	7	13.2	0.040	38	17.2	0.068
8	37.5	0.107	60	32.3	0.137	8	14.1	0.043	39	18.3	0.072
9	35.2	0.101	61	31.3	0.132	9	15.1	0.046	40	19.3	0.076
10	33.3	0.095	62	30.3	0.128	10	16.2	0.049	41	20.3	0.080
11	30.6	0.088	63	29.3	0.124	11	17.2	0.052	42	21.2	0.084
12	28.6	0.082	64	28.3	0.120	12	18.0	0.055	43	22.2	0.088
13	26.5	0.076	65	27.3	0.115	13	19.0	0.057	44	23.2	0.092
14	24.3	0.069	66	26.3	0.111	14	20.0	0.061	45	24.2	0.096
15	22.1	0.063	67	25.3	0.107	15	21.0	0.063	46	25.4	0.100
16	19.9	0.057	68	24.3	0.103	16	21.7	0.066	47	26.4	0.104
17	17.7	0.051	69	23.3	0.098	17	23.0	0.070	48	27.3	0.108
18	15.5	0.044	70	22.3	0.094	18	24.0	0.073	49	28.4	0.112
19	13.2	0.038	71	21.3	0.090	19	25.0	0.076	50	29.4	0.116
20	11.0	0.031	72	20.2	0.086	20	25.9	0.078	51	30.4	0.120
21	8.9	0.025	73	19.3	0.082	21	27.0	0.082	52	31.2	0.123
22	6.5	0.019	74	18.3	0.077	22	27.9	0.084	53	32.2	0.127
23	4.5	0.013	75	17.3	0.073	23	29.1	0.088	54	33.2	0.131
24	204.8	0.585	76	16.3	0.069	24	30.0	0.091	55	34.3	0.136
25	124.5	0.356	77	15.3	0.065	25	31.0	0.094	56	35.4	0.140
26	44.5	0.127	78	14.4	0.061	26	32.0	0.097	57	36.4	0.144
27	5.2	0.015	79	13.4	0.057	27	12.1	0.036	58	21.1	0.083
28	84.4	0.241	80	12.4	0.052	28	32.0	0.097	59	41.1	0.162
29	164.5	0.470	81	11.4	0.048	29	52.0	0.157	60	61.1	0.242
30	53.2	0.160	82	10.3	0.044	30	72.0	0.218	61	81.1	0.321
31	51.0	0.154	83	9.3	0.039	31	92.0	0.278	62	101.1	0.400
32	48.8	0.147									
33	46.6	0.140									
34	44.3	0.134									
35	42.2	0.127									
36	39.9	0.120									
37	37.6	0.113									
38	35.3	0.106									
39	33.1	0.100									
40	30.7	0.092									
41	28.5	0.086									
42	26.3	0.079									
43	24.1	0.073									
44	21.8	0.066									
45	19.7	0.059									
46	17.5	0.053									
47	15.3	0.046									
48	13.1	0.039									
49	10.8	0.033									
50	8.7	0.026									
51	6.4	0.019									
52	4.3	0.013									

[a]Leading edge at FS 162 and FS 172. For orifices 1–29, c = 350.1 (BL 43.5). For orifices 30–52, c = 331.6 (BL 51.0).

[b]Leading edge at FS 263.9; c = 236.7 (BL 89.6).

[c]Leading edge at FS 176.5; c = 330.7 (BL 51.4).

[d]Leading edge at FS 246.5; c = 252.7 (BL 83.1).

Table 2. Orifice locations for pressure belt configuration 1a. (Distance measured from leading edge.)

Upper surface						Lower surface					
Inboard[a]			Outboard[b]			Inboard[c]			Outboard[d]		
Orifice	x in.	x/c	Orifice	x in.	x/c	Orifice	x in.	x/c	Orifice	x in.	x/c
1	53.0	0.151	53	1.6	0.007	1	7.1	0.022	32	11.3	0.045
2	50.7	0.145	54	21.2	0.090	2	8.1	0.025	33	12.3	0.049
3	48.5	0.138	55	41.4	0.175	3	9.1	0.028	34	13.4	0.053
4	46.3	0.132	56	61.3	0.259	4	10.2	0.031	35	14.4	0.057
5	44.0	0.126	57	81.2	0.343	5	11.2	0.034	36	15.3	0.061
6	41.6	0.119	58	34.2	0.145	6	12.2	0.037	37	16.3	0.065
7	39.6	0.113	59	33.2	0.140	7	13.2	0.040	38	17.2	0.068
8	37.5	0.107	60	32.3	0.137	8	14.1	0.043	39	18.3	0.072
9	35.2	0.101	61	31.3	0.132	9	15.1	0.046	40	19.3	0.076
10	33.3	0.095	62	30.3	0.128	10	16.2	0.049	41	20.3	0.080
11	30.6	0.088	63	29.3	0.124	11	17.2	0.052	42	21.2	0.084
12	28.6	0.082	64	28.3	0.120	12	18.0	0.055	43	22.2	0.088
13	26.5	0.076	65	27.3	0.115	13	19.0	0.057	44	23.2	0.092
14	24.3	0.069	66	26.3	0.111	14	20.0	0.061	45	24.2	0.096
15	22.1	0.063	67	25.3	0.107	15	21.0	0.063	46	25.4	0.100
16	19.9	0.057	68	24.3	0.103	16	21.7	0.066	47	26.4	0.104
17	17.7	0.051	69	23.3	0.098	17	23.0	0.070	48	27.3	0.108
18	15.5	0.044	70	22.3	0.094	18	24.0	0.073	49	28.4	0.112
19	13.2	0.038	71	21.3	0.090	19	25.0	0.076	50	29.4	0.116
20	11.0	0.031	72	20.2	0.086	20	25.9	0.078	51	30.4	0.120
21	8.9	0.025	73	19.3	0.082	21	27.0	0.082	52	31.2	0.123
22	6.5	0.019	74	18.3	0.077	22	27.9	0.084	53	32.2	0.127
23	4.5	0.013	75	17.3	0.073	23	29.1	0.088	54	33.2	0.131
24	**5.2**	**0.015**	76	16.3	0.069	24	30.0	0.091	55	34.3	0.136
25	**4.5**	**0.127**	77	15.3	0.065	25	31.0	0.094	56	35.4	0.140
26	**84.44**	**0.241**	78	14.4	0.061	26	32.0	0.097	57	36.4	0.144
27	**124.5**	**0.356**	79	13.4	0.057	27	12.1	0.036	58	21.1	0.083
28	**164.5**	**0.470**	80	12.4	0.052	28	32.0	0.097	59	41.1	0.162
29	**204.8**	**0.585**	81	11.4	0.048	29	52.0	0.157	60	61.1	0.242
30	53.2	0.160	82	10.3	0.044	30	72.0	0.218	61	81.1	0.321
31	51.0	0.154	83	9.3	0.039	31	92.0	0.278	62	101.1	0.400
32	48.8	0.147									
33	46.6	0.140									
34	44.3	0.134									
35	42.2	0.127									
36	39.9	0.120									
37	37.6	0.113									
38	35.3	0.106									
39	33.1	0.100									
40	30.7	0.092									
41	28.5	0.086									
42	26.3	0.079									
43	24.1	0.073									
44	21.8	0.066									
45	19.7	0.059									
46	17.5	0.053									
47	15.3	0.046									
48	13.1	0.039									
49	10.8	0.033									
50	8.7	0.026									
51	6.4	0.019									
52	4.3	0.013									

[a]Leading edge at FS 162 and FS 172. For orifices 1–29, c = 350.1 (BL 43.5). For orifices 30–52, c = 331.6 (BL 51.0).

[b]Leading edge at FS 263.9; c = 236.7 (BL 89.6).

[c]Leading edge at FS 176.5; c = 330.7 (BL 51.4).

[d]Leading edge at FS 246.5; c = 252.7 (BL 83.1).

Table 3. Orifice locations for pressure belt configuration 2. (Distance measured from leading edge.)

Upper surface						Lower surface					
Inboard[a]			Outboard[b]			Inboard[c]			Outboard[d]		
Orifice	x in.	x/c	Orifice	x in.	x/c	Orifice	x in.	x/c	Orifice	x in.	x/c
1	103.6	0.296	53	1.6	0.007	1	7.1	0.022	32	11.3	0.045
2	101.4	0.29	54	21.2	0.09	2	8.1	0.025	33	12.3	0.049
3	99.2	0.283	55	41.4	0.175	3	9.1	0.028	34	13.4	0.053
4	97	0.277	56	61.3	0.259	4	10.2	0.031	35	14.4	0.057
5	94.8	0.271	57	81.2	0.343	5	11.2	0.034	36	15.3	0.061
6	92.6	0.265	58	69.3	0.293	6	12.2	0.037	37	16.3	0.065
7	90.4	0.258	59	68.3	0.289	7	13.2	0.04	38	17.2	0.068
8	88.2	0.252	60	67.3	0.284	8	14.1	0.043	39	18.3	0.072
9	86	0.246	61	66.3	0.28	9	15.1	0.046	40	19.3	0.076
10	83.8	0.239	62	65.3	0.276	10	16.2	0.049	41	20.3	0.08
11	81.6	0.233	63	64.3	0.272	11	17.2	0.052	42	21.2	0.084
12	79.4	0.227	64	63.3	0.267	12	18	0.055	43	22.2	0.088
13	77.2	0.221	65	62.3	0.263	13	19	0.057	44	23.2	0.092
14	75	0.214	66	61.3	0.259	14	20	0.061	45	24.2	0.096
15	72.8	0.208	67	60.3	0.255	15	21	0.063	46	25.4	0.1
16	70.6	0.202	68	59.3	0.251	16	21.7	0.066	47	26.4	0.104
17	68.4	0.195	69	58.3	0.246	17	23	0.07	48	27.3	0.108
18	66.2	0.189	70	57.3	0.242	18	24	0.073	49	28.4	0.112
19	64	0.183	71	56.3	0.238	19	25	0.076	50	29.4	0.116
20	61.8	0.176	72	55.3	0.234	20	25.9	0.078	51	30.4	0.12
21	59.6	0.17	73	54.3	0.229	21	27	0.082	52	31.2	0.123
22	57.4	0.164	74	53.3	0.225	22	27.9	0.084	53	32.2	0.127
23	55.2	0.158	75	52.3	0.221	23	29.1	0.088	54	33.2	0.131
24	5.2	0.015	76	51.3	0.217	24	30	0.091	55	34.3	0.136
25	4.5	0.127	77	50.3	0.212	25	31	0.094	56	35.4	0.14
26	84.44	0.241	78	49.3	0.208	26	32	0.097	57	36.4	0.144
27	124.5	0.356	79	48.3	0.204	27	12.1	0.036	58	21.1	0.083
28	164.5	0.47	80	47.3	0.2	28	32	0.097	59	41.1	0.162
29	204.8	0.585	81	46.3	0.196	29	52	0.157	60	61.1	0.242
30	103.8	0.313	82	45.3	0.191	30	72	0.218	61	81.1	0.321
31	101.6	0.306	83	44.3	0.187	31	92	0.278	62	101.1	0.4
32	99.4	0.25									
33	97.2	0.293									
34	95	0.287									
35	92.8	0.28									
36	90.6	0.273									
37	88.4	0.266									
38	86.2	0.26									
39	84	0.253									
40	81.8	0.247									
41	79.6	0.24									
42	77.4	0.233									
43	75.2	0.227									
44	73	0.22									
45	70.8	0.214									
46	68.6	0.207									
47	66.4	0.2									
48	64.2	0.194									
49	62	0.187									
50	59.8	0.18									
51	57.6	0.174									
52	55.4	0.167									

[a]Leading edge at FS 162 and FS 172. For orifices 1–29, c = 350.1 (BL 43.5). For orifices 30–52, c = 331.6 (BL 51.0).

[b]Leading edge at FS 263.9; c = 236.7 (BL 89.6).

[c]Leading edge at FS 176.5; c = 330.7 (BL 51.4).

[d]Leading edge at FS 246.5; c = 252.7 (BL 83.1).

Table 4. Orifice locations for pressure belt configuration 2b. (Distance measured from leading edge.)

Upper surface						Lower surface					
Inboard[a]			Outboard[b]			Inboard[c]			Outboard[d]		
Orifice	x in.	x/c	Orifice	x in.	x/c	Orifice	x in.	x/c	Orifice	x in.	x/c
1	103.6	0.296	53	1.6	0.007	1	7.1	0.022	32	2.8	0.009
2	101.4	0.29	54	21.2	0.09	2	8.1	0.025	33	3.8	0.012
3	99.2	0.283	55	41.4	0.175	3	9.1	0.028	34	4.8	0.015
4	97	0.277	56	61.3	0.259	4	10.2	0.031	35	5.8	0.019
5	94.8	0.271	57	81.2	0.343	5	11.2	0.034	36	6.8	0.022
6	92.6	0.265	58	69.3	0.293	6	12.2	0.037	37	7.8	0.025
7	90.4	0.258	59	68.3	0.289	7	13.2	0.04	38	8.8	0.028
8	88.2	0.252	60	67.3	0.284	8	14.1	0.043	39	9.8	0.031
9	86	0.246	61	66.3	0.28	9	15.1	0.046	40	10.8	0.035
10	83.8	0.239	62	65.3	0.276	10	16.2	0.049	41	11.8	0.038
11	81.6	0.233	63	64.3	0.272	11	17.2	0.052	42	12.8	0.041
12	79.4	0.227	64	63.3	0.267	12	18	0.055	43	13.8	0.044
13	77.2	0.221	65	62.3	0.263	13	19	0.057	44	14.8	0.048
14	75	0.214	66	61.3	0.259	14	20	0.061	45	15.8	0.051
15	72.8	0.208	67	60.3	0.255	15	21	0.063	46	16.8	0.054
16	70.6	0.202	68	59.3	0.251	16	21.7	0.066	47	18.8	0.06
17	68.4	0.195	69	58.3	0.246	17	23	0.07	48	19.8	0.064
18	66.2	0.189	70	57.3	0.242	18	24	0.073	49	20.8	0.067
19	64	0.183	71	56.3	0.238	19	25	0.076	50	21.8	0.07
20	61.8	0.176	72	55.3	0.234	20	25.9	0.078	51	22.8	0.073
21	59.6	0.17	73	54.3	0.229	21	27	0.082	52	23.8	0.076
22	57.4	0.164	74	53.3	0.225	22	27.9	0.084	53	24.8	0.08
23	55.2	0.158	75	52.3	0.221	23	29.1	0.088	54	25.8	0.083
24	5.2	0.015	76	51.3	0.217	24	30	0.091	55	3.3	0.011
25	4.5	0.127	77	50.3	0.212	25	31	0.094	56	4.8	0.016
26	84.44	0.241	78	49.3	0.208	26	32	0.097	57	6.3	0.021
27	124.5	0.356	79	48.3	0.204	27	12.1	0.036	58	7.8	0.026
28	164.5	0.47	80	47.3	0.2	28	32	0.097	59	9.3	0.031
29	204.8	0.585	81	46.3	0.196	29	52	0.157	60	10.8	0.036
30	103.8	0.313	82	45.3	0.191	30	72	0.218	61	12.3	0.041
31	101.6	0.306	83	44.3	0.187	31	92	0.278	62	14.8	0.046
32	99.4	0.25									
33	97.2	0.293									
34	95	0.287									
35	92.8	0.28									
36	90.6	0.273									
37	88.4	0.266									
38	86.2	0.26									
39	84	0.253									
40	81.8	0.247									
41	79.6	0.24									
42	77.4	0.233									
43	75.2	0.227									
44	73	0.22									
45	70.8	0.214									
46	68.6	0.207									
47	66.4	0.2									
48	64.2	0.194									
49	62	0.187									
50	59.8	0.18									
51	57.6	0.174									
52	55.4	0.167									

[a]Leading edge at FS 162 and FS 172. For orifices 1–29, c = 350.1 (BL 43.5). For orifices 30–52, c = 331.6 (BL 51.0).

[b]Leading edge at FS 263.9; c = 236.7 (BL 89.6).

[c]Leading edge at FS 176.5; c = 330.7 (BL 51.4).

[d]Leading edge at FS 246.5; c = 252.7 (BL 83.1).

Table 5. Orifice locations for pressure belt configuration 3. (Distance measured from leading edge.)

Upper surface						Lower surface					
Inboard[a]			Outboard[b]			Inboard[c]			Outboard[d]		
Orifice	*x* in.	*x/c*	Orifice	*x* in.	*x/c*	Orifice	*x* in.	*x/c*	Orifice	*x* in.	*x/c*
1	154.4	0.441	53	1.6	0.007	1	7.1	0.022	32	2.8	0.009
2	152.2	0.435	54	21.2	0.09	2	8.1	0.025	33	3.8	0.012
3	150	0.428	55	41.4	0.175	3	9.1	0.028	34	4.8	0.015
4	147.8	0.422	56	61.3	0.259	4	10.2	0.031	35	5.8	0.019
5	145.6	0.416	57	81.2	0.343	5	11.2	0.034	36	6.8	0.022
6	143.4	0.409	58	95.6	0.404	6	12.2	0.037	37	7.8	0.025
7	141.2	0.403	59	94.6	0.4	7	13.2	0.04	38	8.8	0.028
8	139	0.397	60	93.6	0.395	8	14.1	0.043	39	9.8	0.031
9	136.8	0.391	61	92.6	0.391	9	15.1	0.046	40	10.8	0.035
10	134.6	0.384	62	91.6	0.387	10	16.2	0.049	41	11.8	0.038
11	132.4	0.378	63	90.6	0.383	11	17.2	0.052	42	12.8	0.041
12	130.2	0.372	64	89.6	0.378	12	18	0.055	43	13.8	0.044
13	128	0.365	65	88.6	0.374	13	19	0.057	44	14.8	0.048
14	125.8	0.359	66	87.6	0.37	14	20	0.061	45	15.8	0.051
15	123.6	0.353	67	86.6	0.366	15	21	0.063	46	16.8	0.054
16	121.4	0.347	68	85.6	0.362	16	21.7	0.066	47	18.8	0.06
17	119.2	0.34	69	84.6	0.357	17	23	0.07	48	19.8	0.064
18	117	0.334	70	83.6	0.353	18	24	0.073	49	20.8	0.067
19	114.8	0.327	71	82.6	0.349	19	25	0.076	50	21.8	0.07
20	112.6	0.321	72	81.6	0.345	20	25.9	0.078	51	22.8	0.073
21	110.4	0.315	73	80.6	0.341	21	27	0.082	52	23.8	0.076
22	108.2	0.309	74	79.6	0.336	22	27.9	0.084	53	24.8	0.08
23	106	0.303	75	78.6	0.332	23	29.1	0.088	54	25.8	0.083
24	5.2	0.015	76	77.6	0.328	24	30	0.091	55	3.3	0.011
25	4.5	0.127	77	76.6	0.324	25	31	0.094	56	4.8	0.016
26	84.44	0.241	78	75.6	0.319	26	32	0.097	57	6.3	0.021
27	124.5	0.356	79	74.6	0.315	27	12.1	0.036	58	7.8	0.026
28	164.5	0.47	80	73.6	0.311	28	32	0.097	59	9.3	0.031
29	204.8	0.585	81	72.6	0.307	29	52	0.157	60	10.8	0.036
30	154.2	0.465	82	71.6	0.306	30	72	0.218	61	12.3	0.041
31	152	0.458	83	70.6	0.298	31	92	0.278	62	14.8	0.046
32	149.8	0.452									
33	147.6	0.445									
34	145.4	0.438									
35	143.2	0.432									
36	141	0.425									
37	138.8	0.419									
38	136.6	0.412									
39	134.4	0.405									
40	132.2	0.399									
41	130	0.392									
42	127.8	0.385									
43	125.6	0.379									
44	123.4	0.372									
45	121.2	0.366									
46	119	0.359									
47	116.8	0.352									
48	114.6	0.346									
49	112.4	0.339									
50	110.2	0.332									
51	108	0.326									
52	105.8	0.319									

[a]Leading edge at FS 162 and FS 172. For orifices 1–29, c = 350.1 (BL 43.5). For orifices 30–52, c = 331.6 (BL 51.0).

[b]Leading edge at FS 263.9; c = 236.7 (BL 89.6).

[c]Leading edge at FS 176.5; c = 330.7 (BL 51.4).

[d]For orifices 32–54 c = 310.7 (BL 59.6). For orifices 55–62 c = 301.8 (BL 63.1).

Table 6. Orifice locations for pressure belt configuration 4. (Distance measured from leading edge.)

Upper surface						Lower surface					
Inboard[a]			Outboard[b]			Inboard[c]			Outboard[d]		
Orifice	x in.	x/c	Orifice	x in.	x/c	Orifice	x in.	x/c	Orifice	x in.	x/c
1	205	0.585	53	1.6	0.007	1	7.1	0.022	32	2.8	0.009
2	202.8	0.579	54	21.2	0.09	2	8.1	0.025	33	3.8	0.012
3	200.6	0.573	55	41.4	0.175	3	9.1	0.028	34	4.8	0.015
4	198.4	0.566	56	61.3	0.259	4	10.2	0.031	35	5.8	0.019
5	196.2	0.56	57	81.2	0.343	5	11.2	0.034	36	6.8	0.022
6	194	0.554	58	121.6	0.514	6	12.2	0.037	37	7.8	0.025
7	191.8	0.548	59	120.6	0.509	7	13.2	0.04	38	8.8	0.028
8	189.6	0.541	60	119.6	0.505	8	14.1	0.043	39	9.8	0.031
9	187.4	0.535	61	118.6	0.501	9	15.1	0.046	40	10.8	0.035
10	185.2	0.529	62	117.6	0.497	10	16.2	0.049	41	11.8	0.038
11	183	0.523	63	116.6	0.493	11	17.2	0.052	42	12.8	0.041
12	180.8	0.516	64	115.6	0.488	12	18	0.055	43	13.8	0.044
13	178.6	0.51	65	114.6	0.484	13	19	0.057	44	14.8	0.048
14	176.4	0.504	66	113.6	0.48	14	20	0.061	45	15.8	0.051
15	174.2	0.497	67	112.6	0.476	15	21	0.063	46	16.8	0.054
16	172	0.491	68	111.6	0.471	16	21.7	0.066	47	18.8	0.06
17	169.8	0.485	69	110.6	0.467	17	23	0.07	48	19.8	0.064
18	167.6	0.479	70	109.6	0.463	18	24	0.073	49	20.8	0.067
19	165.4	0.472	71	108.6	0.459	19	25	0.076	50	21.8	0.07
20	163.2	0.466	72	107.6	0.455	20	25.9	0.078	51	22.8	0.073
21	161	0.46	73	106.6	0.45	21	27	0.082	52	23.8	0.076
22	158.8	0.453	74	105.6	0.446	22	27.9	0.084	53	24.8	0.08
23	156.6	0.447	75	104.6	0.442	23	29.1	0.088	54	25.8	0.083
24	5.2	0.015	76	103.6	0.438	24	30	0.091	55	3.3	0.011
25	4.5	0.127	77	102.6	0.434	25	31	0.094	56	4.8	0.016
26	84.44	0.241	78	101.6	0.429	26	32	0.097	57	6.3	0.021
27	124.5	0.356	79	100.6	0.425	27	12.1	0.036	58	7.8	0.026
28	164.5	0.47	80	99.6	0.421	28	32	0.097	59	9.3	0.031
29	204.8	0.585	81	98.6	0.417	29	52	0.157	60	10.8	0.036
30	204.8	0.618	82	97.6	0.412	30	72	0.218	61	12.3	0.041
31	202.6	0.611	83	96.6	0.408	31	92	0.278	62	14.8	0.046
32	200.4	0.604									
33	198.2	0.598									
34	196	0.591									
35	193.8	0.584									
36	191.6	0.578									
37	189.4	0.571									
38	187.2	0.565									
39	185	0.558									
40	182.8	0.551									
41	180.6	0.545									
42	178.4	0.538									
43	176.2	0.531									
44	174	0.525									
45	171.8	0.518									
46	169.6	0.511									
47	167.4	0.505									
48	165.2	0.498									
49	163	0.491									
50	160.8	0.485									
51	158.6	0.478									
52	156.4	0.472									

[a]Leading edge at FS 162 and FS 172. For orifices 1–29, c = 350.1 (BL 43.5). For orifices 30–52, c = 331.6 (BL 51.0).

[b]Leading edge at FS 263.9; c = 236.7 (BL 89.6).

[c]Leading edge at FS 176.5; c = 330.7 (BL 51.4).

[d]For orifices 32–54 c = 310.7 (BL 59.6). For orifices 55–62 c – 301.8 (BL 63.1).

Table 7. Configuration time line.

Flight	Date	Configuration	Upper inboard	Upper outboard	Belts lower inboard	Lower outboard	Lower outboard 2	Shock fence	Gun trough fairing
29	19 Apr 93	1	√	√	√	√			
30	21 May 93	1	√	√		√			
31	9 Jun 93	2				√			
32	11 Jun 93	2				√			
33	18 Jun 93	2				√		√	
34	23 Jun 93	1a	√	√	√	√		√	√
35	25 Jun 93	2	√	√	√	√		√	√
36	2 Jul 93	2b	√	√	√		√	√	√
37	7 Jul 93	3	√	√	√		√		√
38	12 Jul 93	3	√	√	√		√		√
39	15 Jul 93	3	√	√	√		√		√
40	21 Jul 93	4	√	√	√		√		√
41	28 Jul 93	4	√	√	√		√		√
42	28 Jul 93	4	√	√	√		√		√
43	30 Jul 93	4	√	√	√		√		√

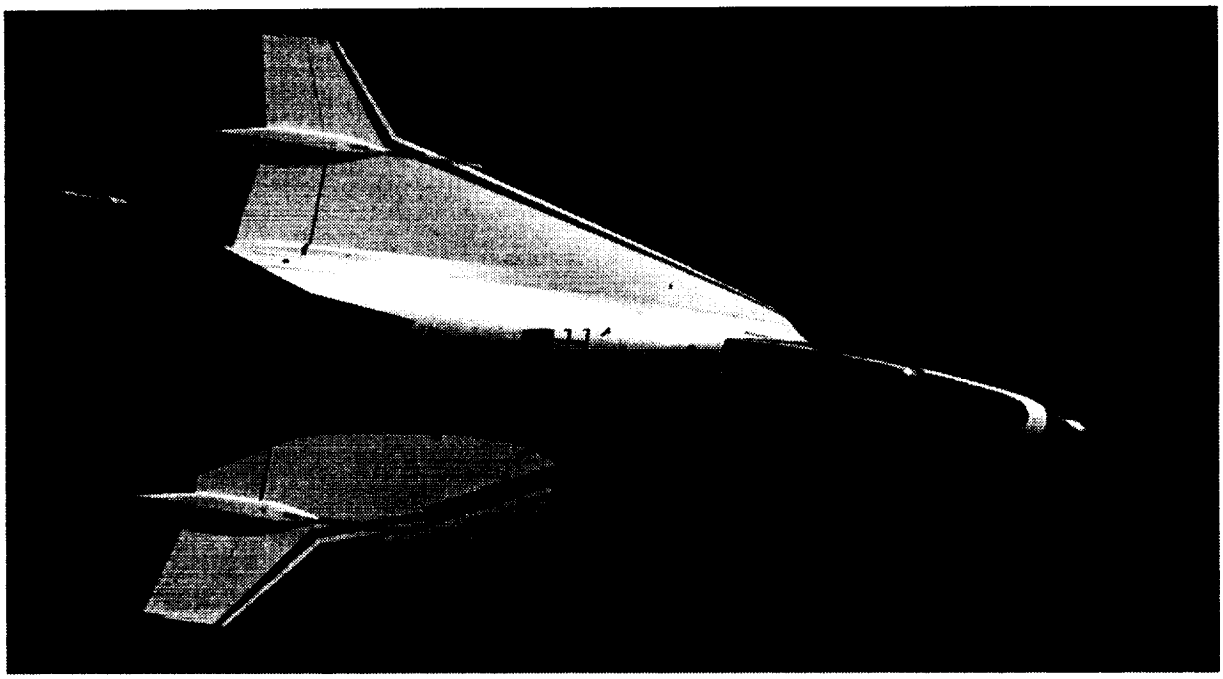

EC93-01286-1

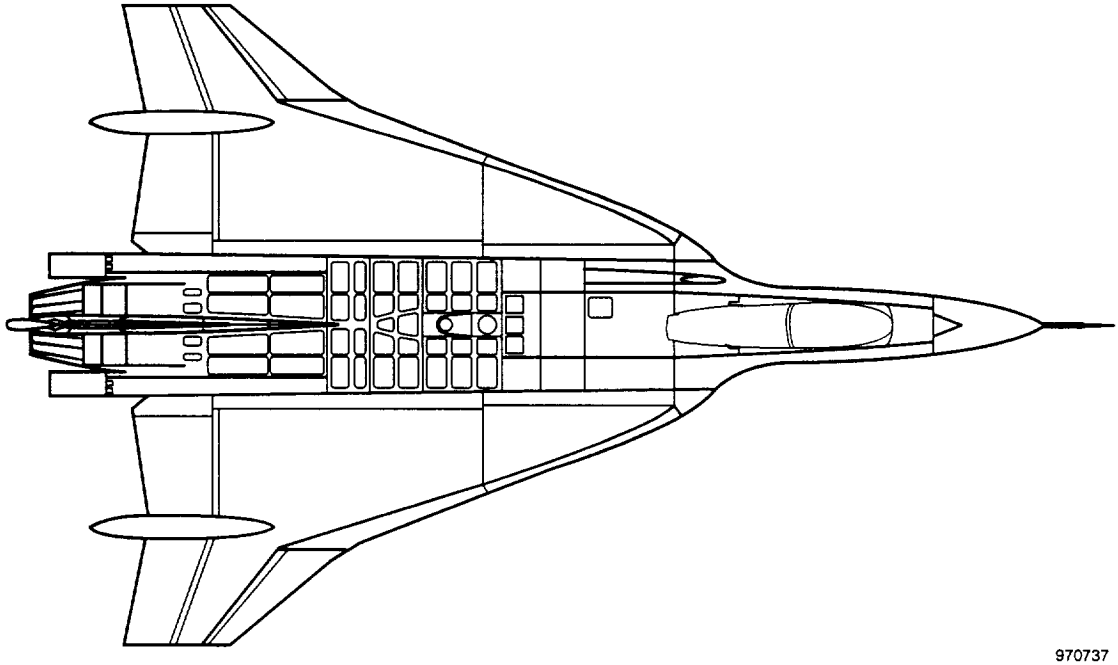

970737

Figure 1. The F-16XL ship 2 planform.

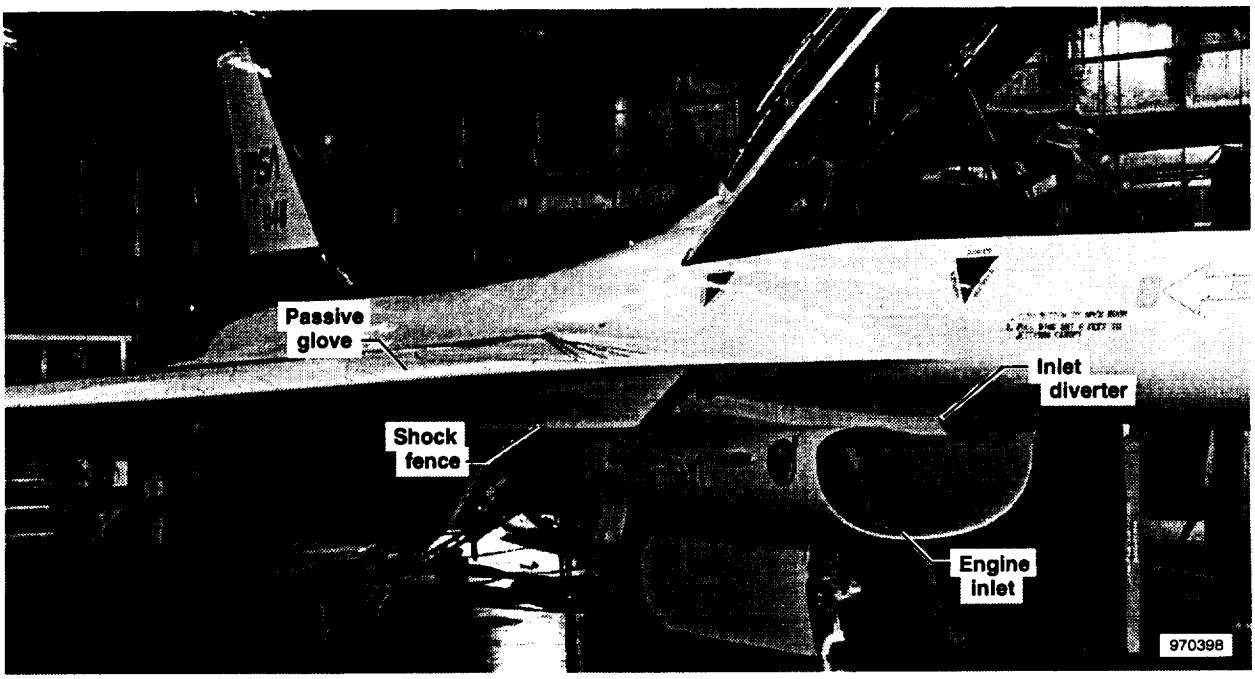

(a) Three-fourth view.

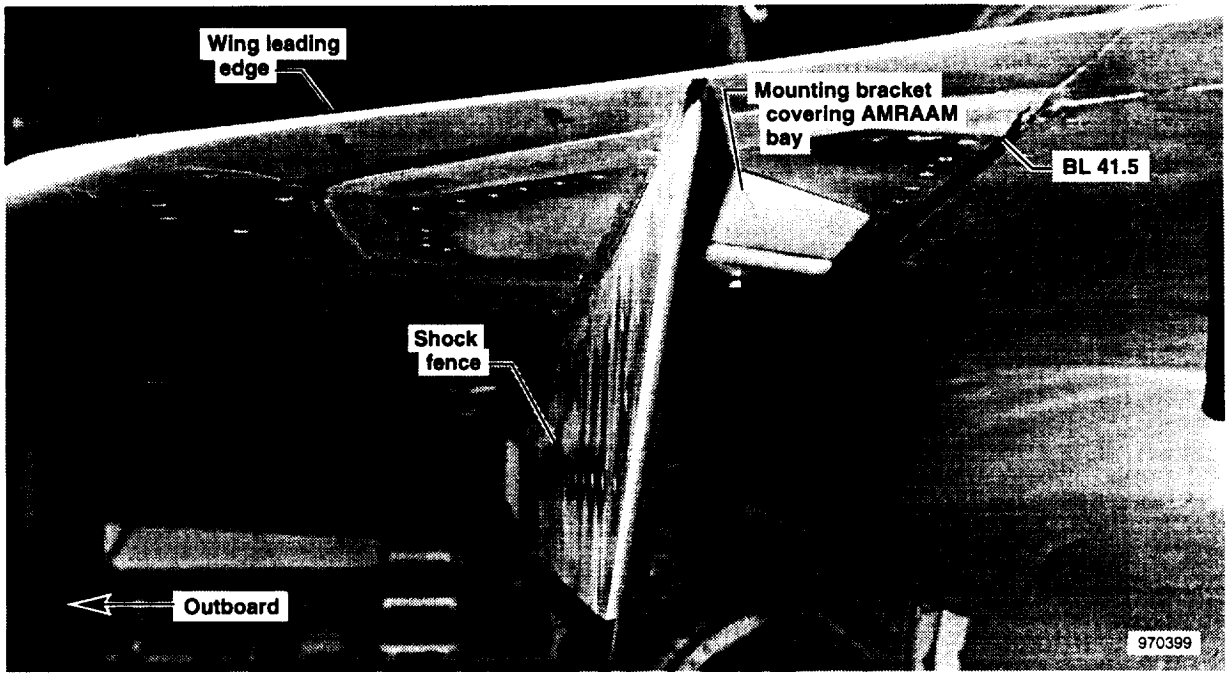

(b) Front view.

Figure 2. Right wing shock fence installation.

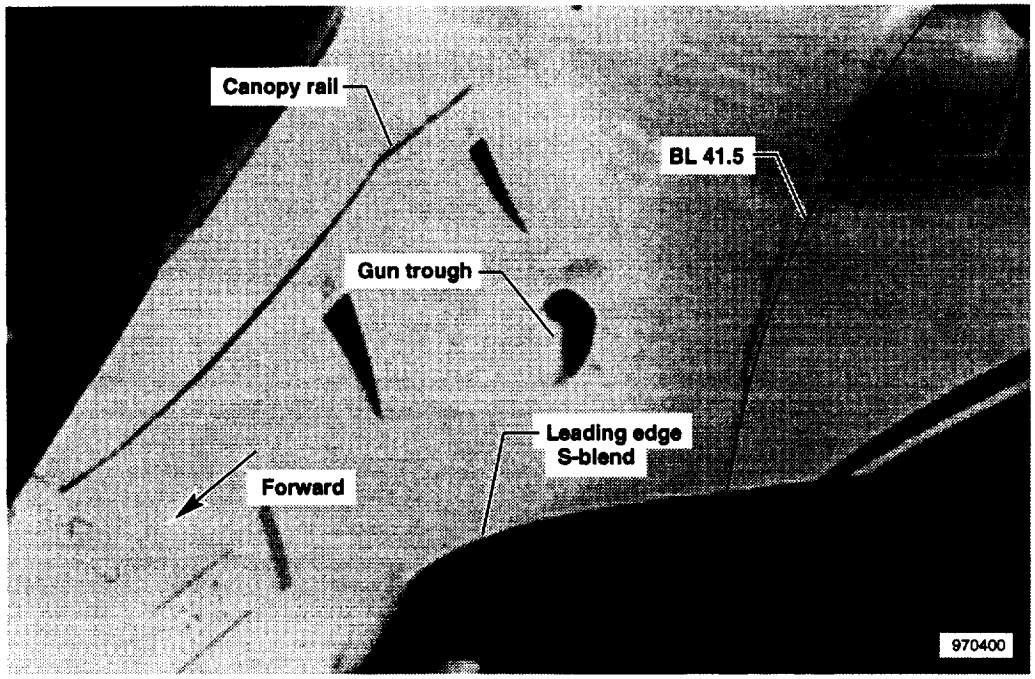

(a) Exposed gun trough on the left side wing root.

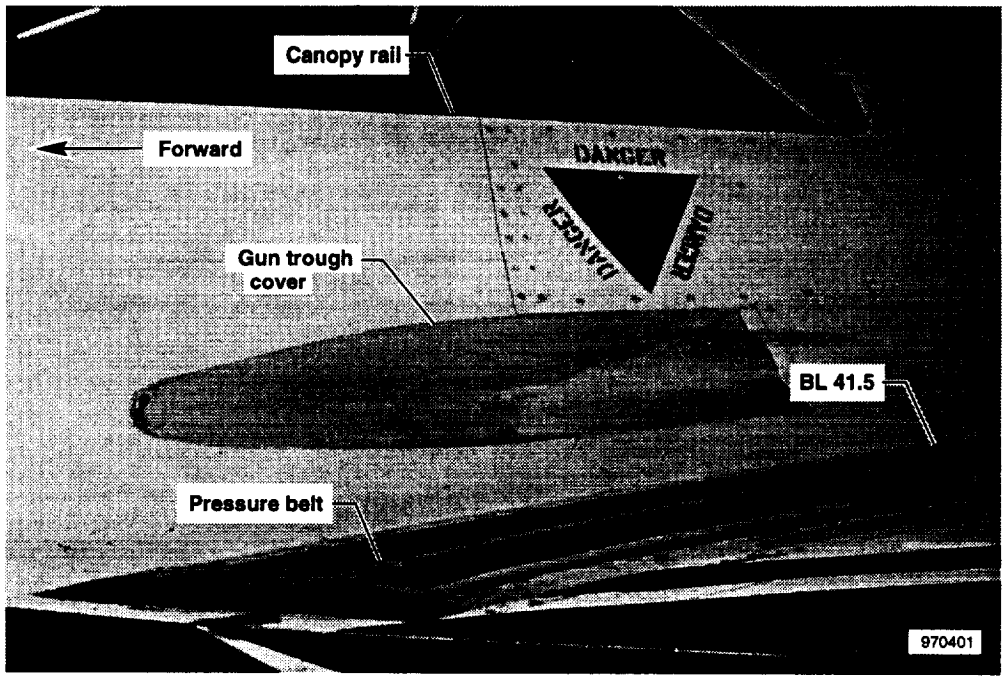

(b) Side view of the faired over gun trough with pressure belts.

Figure 3. Open and faired gun trough.

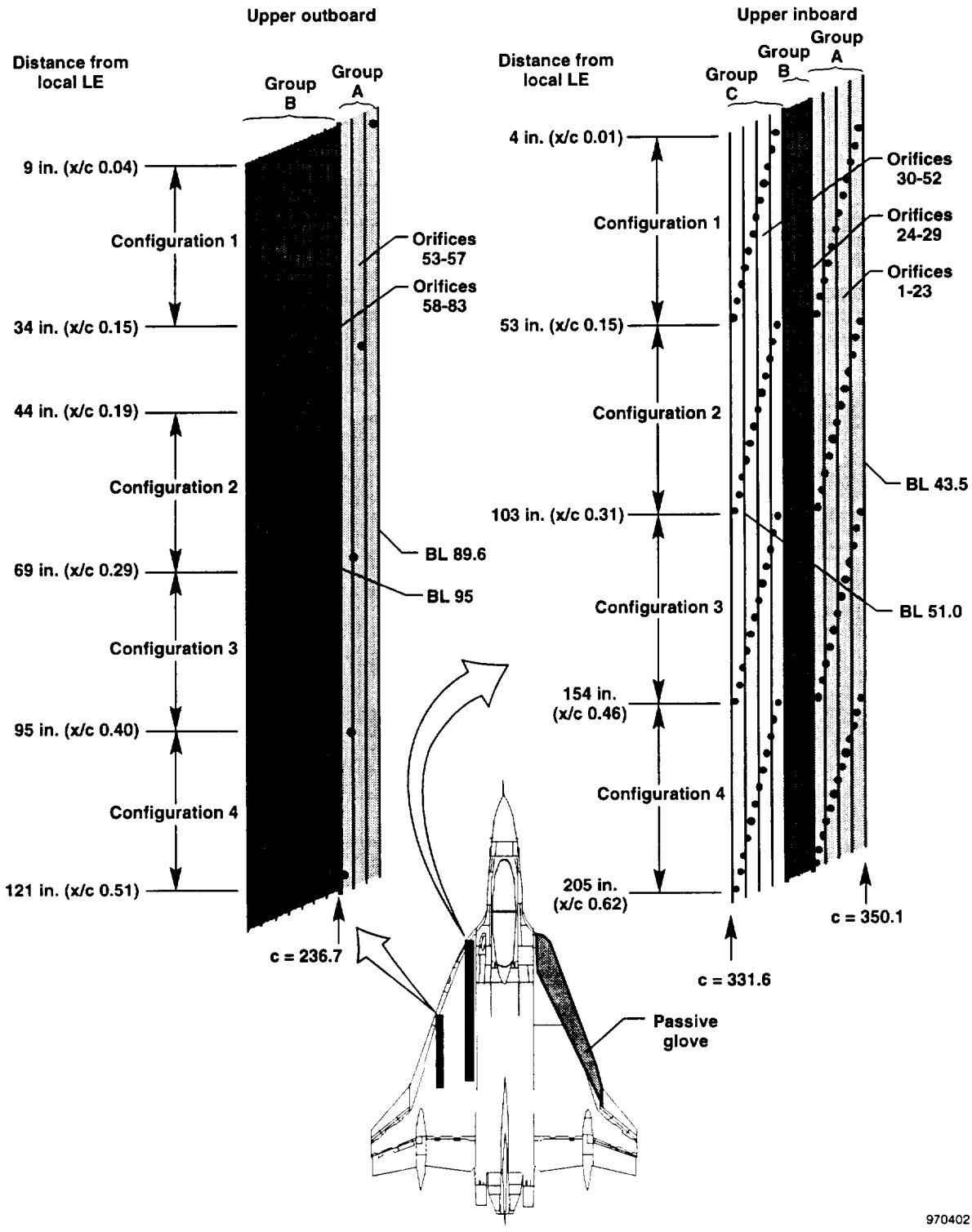

(a) Upper surface.

Figure 4. Pressure belt layout.

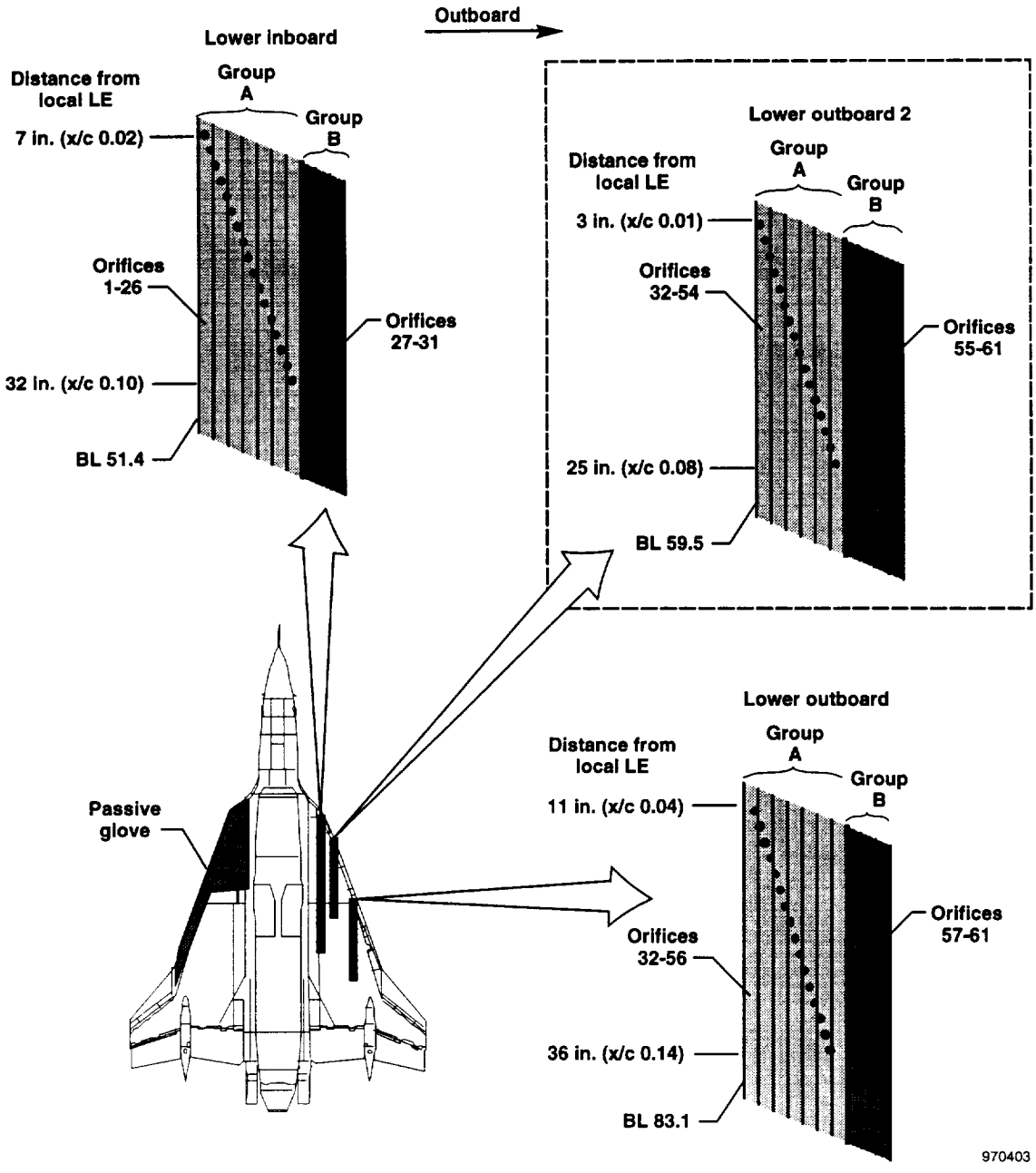

(b) Lower surface.

Figure 4. Continued.

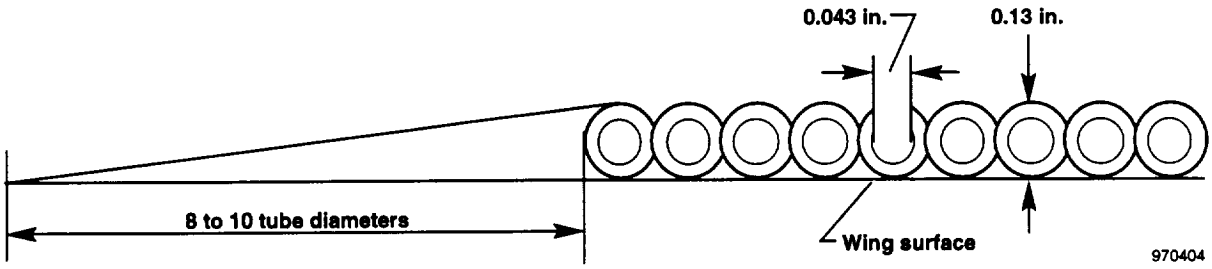

(c) Cross-section of pressure belt mounting with ramp.

Figure 4. Concluded.

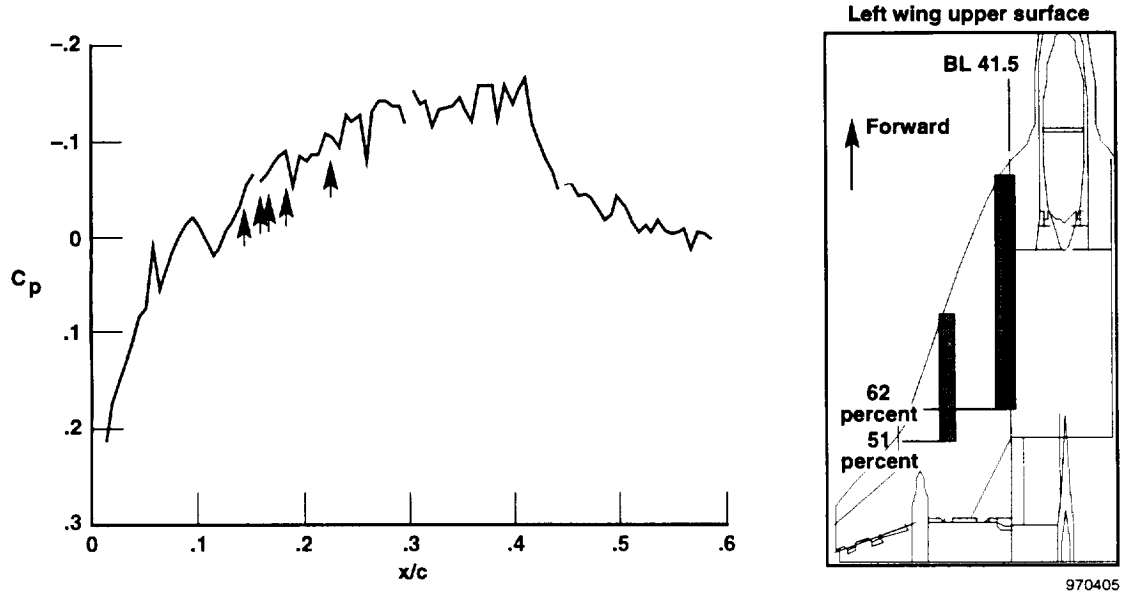

Figure 5. Composite plot showing where sections of the pressure belts lifted up during flight at Mach 1.9, an altitude of 50,000 ft, and an angle of attack of 3.5°. Upper inboard pressure belt group A.

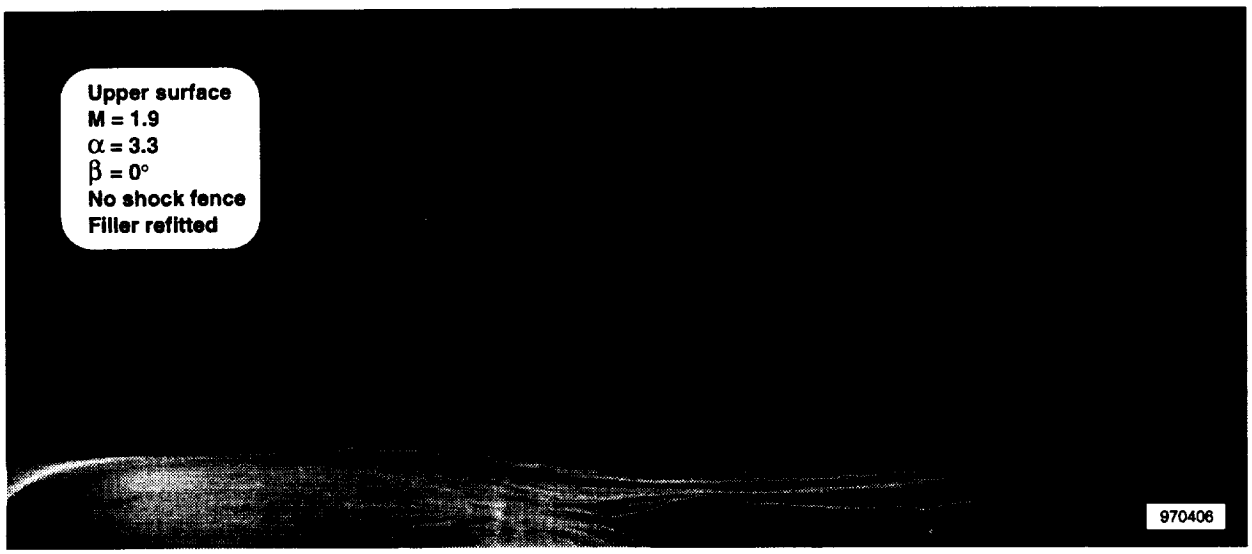

Figure 6. Oil flow photograph taken at Mach 1.9 and at an angle of attack of 3.3° in the NASA Langley Research Center Unitary Plan Supersonic Wind Tunnel.

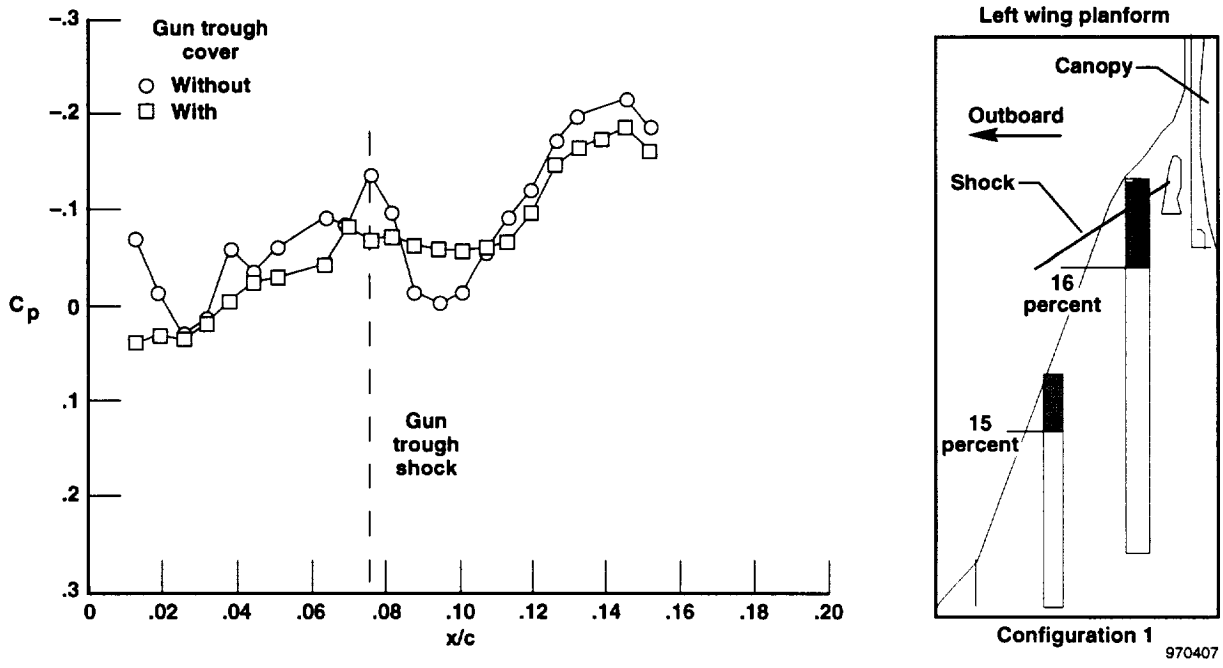

(a) Upper inboard pressure belt, group A.

Figure 7. Upper surface pressures showing gun trough shock at Mach 1.4, an altitude of 46,000 ft, and an angle of attack of 5.2°.

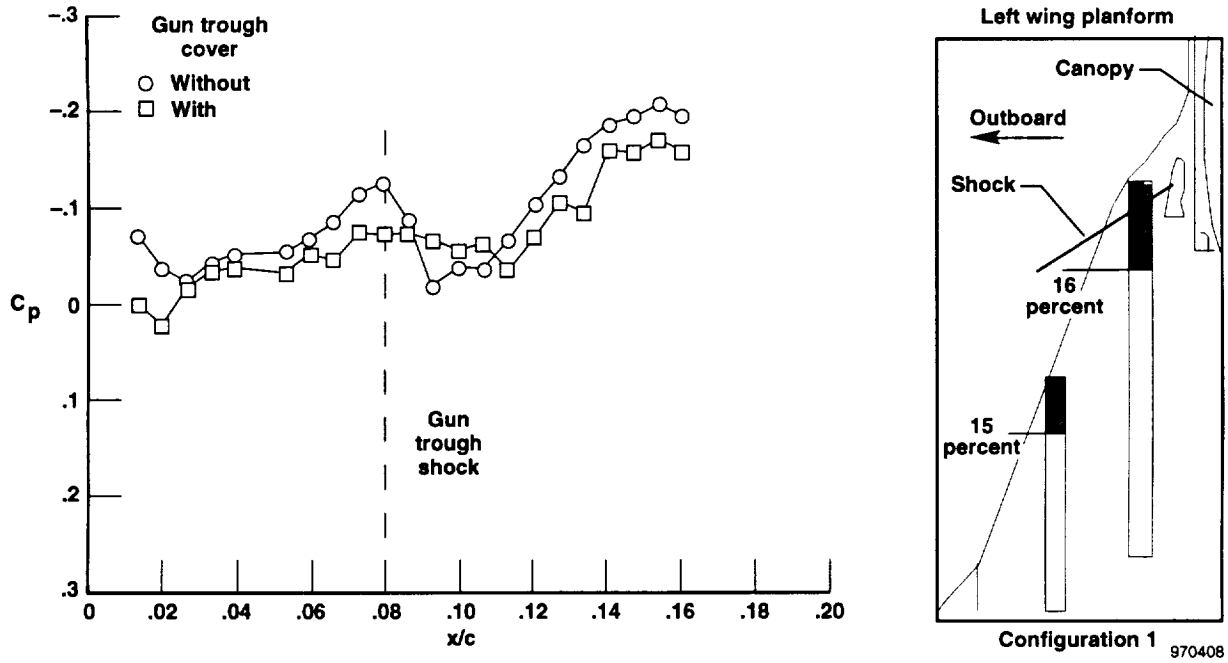

(b) Upper inboard pressure belt, group C.

Figure 7. Concluded.

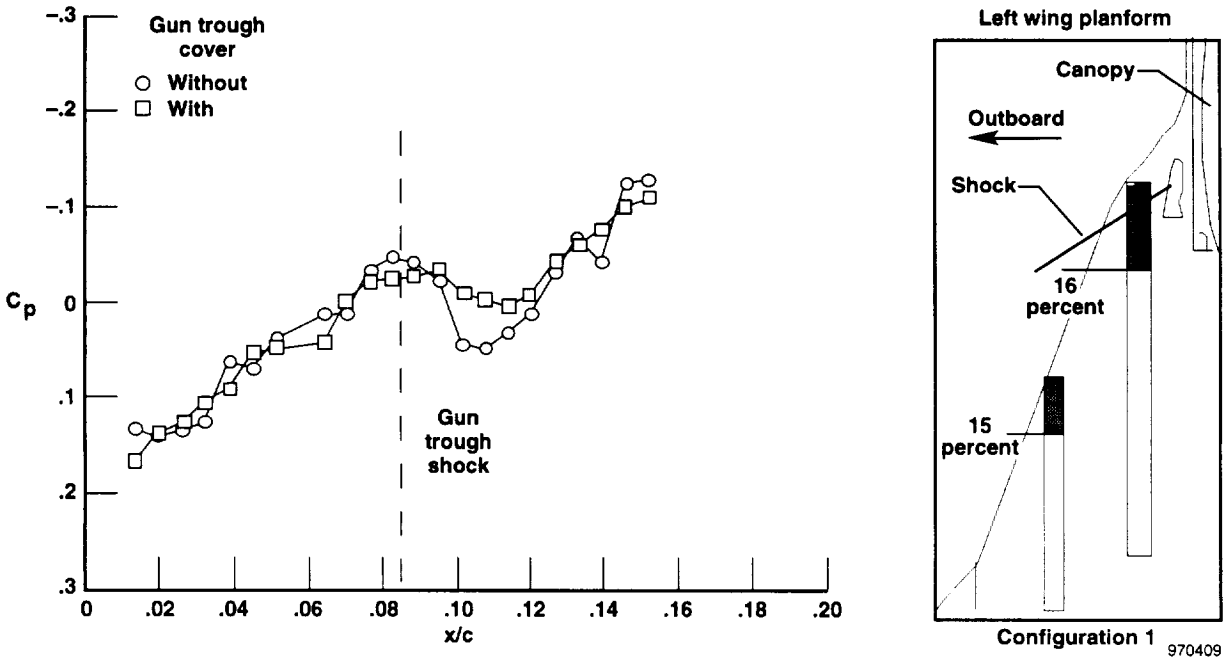

Figure 8. Gun trough shock at Mach 1.7, an altitude of 46,000 ft, and trim angles of attack of 4.0°. Upper inboard pressure belt group A.

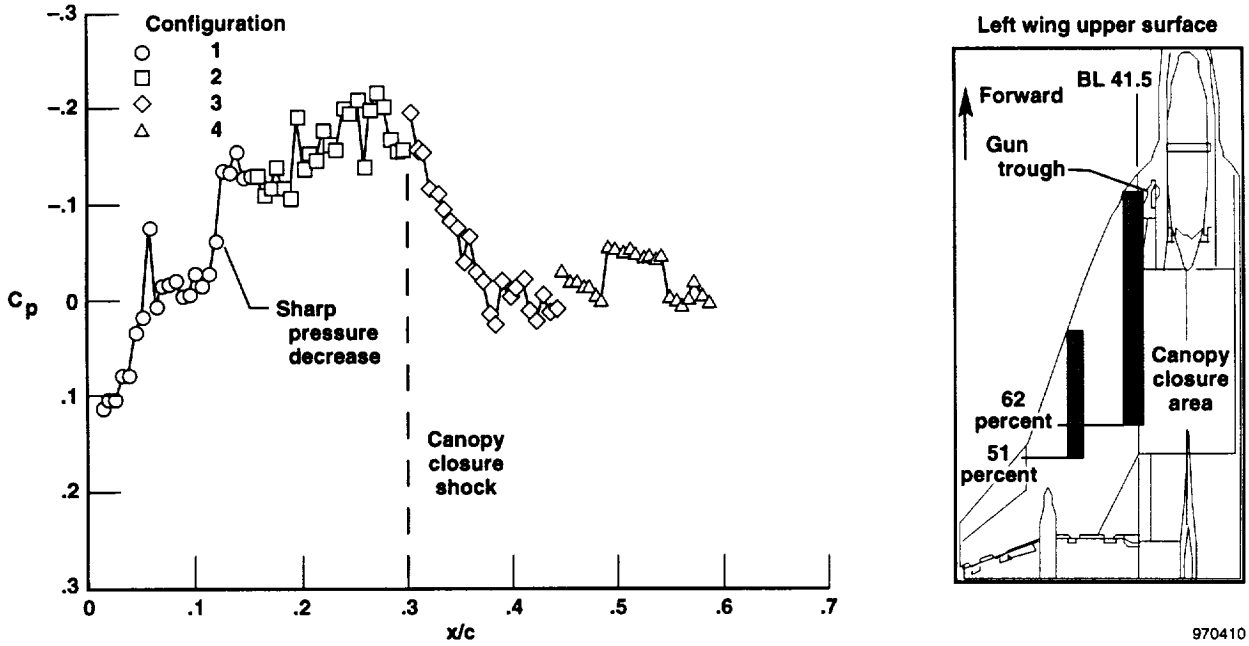

(a) Upper inboard pressure belt, group A.

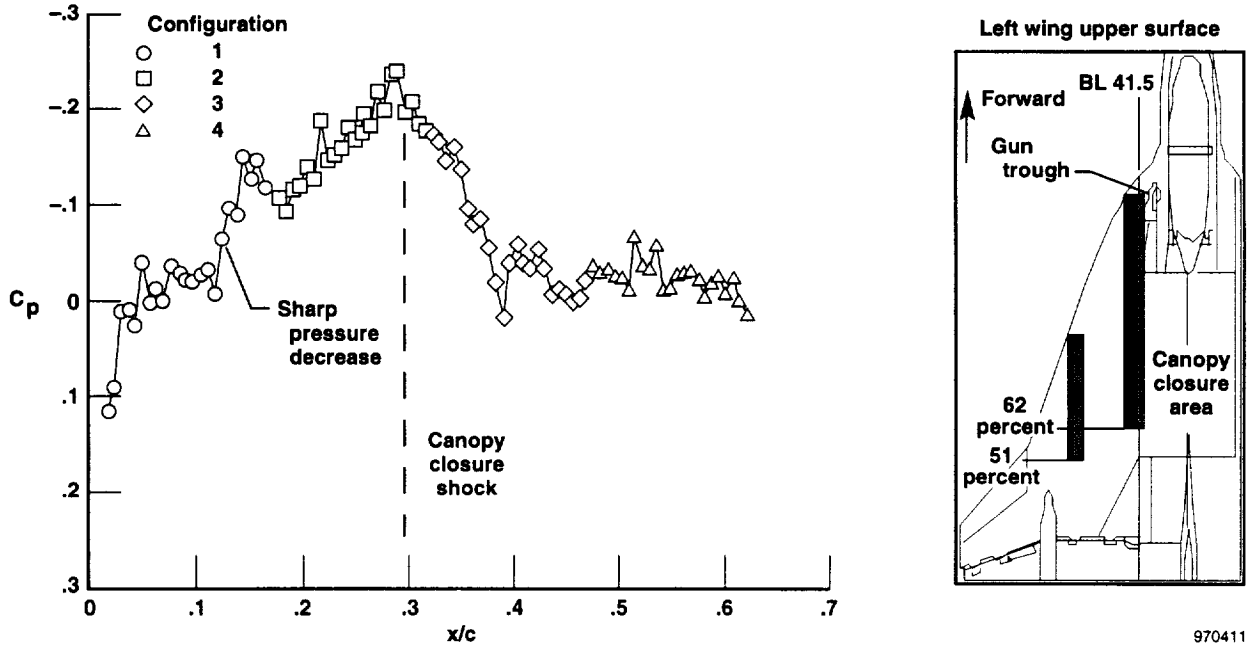

(b) Upper inboard pressure belt, group C.

Figure 9. Composite plot of upper surface pressures with gun trough cover at Mach 1.4, an altitude of 50,000 ft, and an angle of attack of 3.2°.

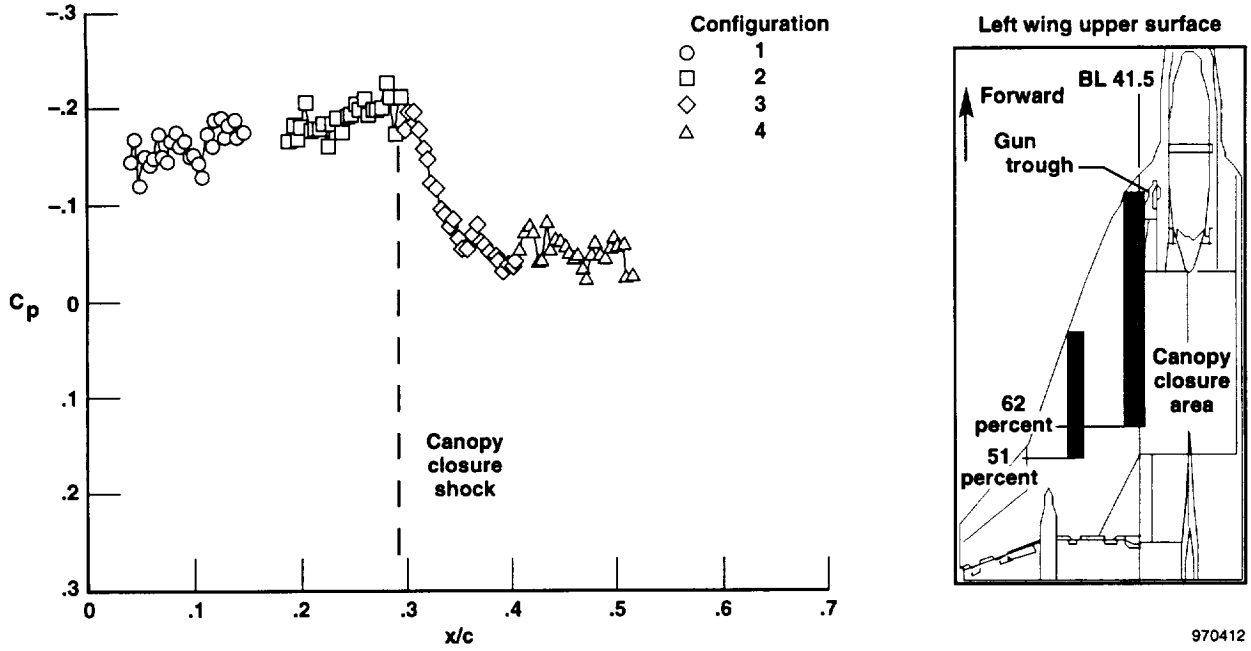

(c) Upper outboard pressure belt.

Figure 9. Concluded.

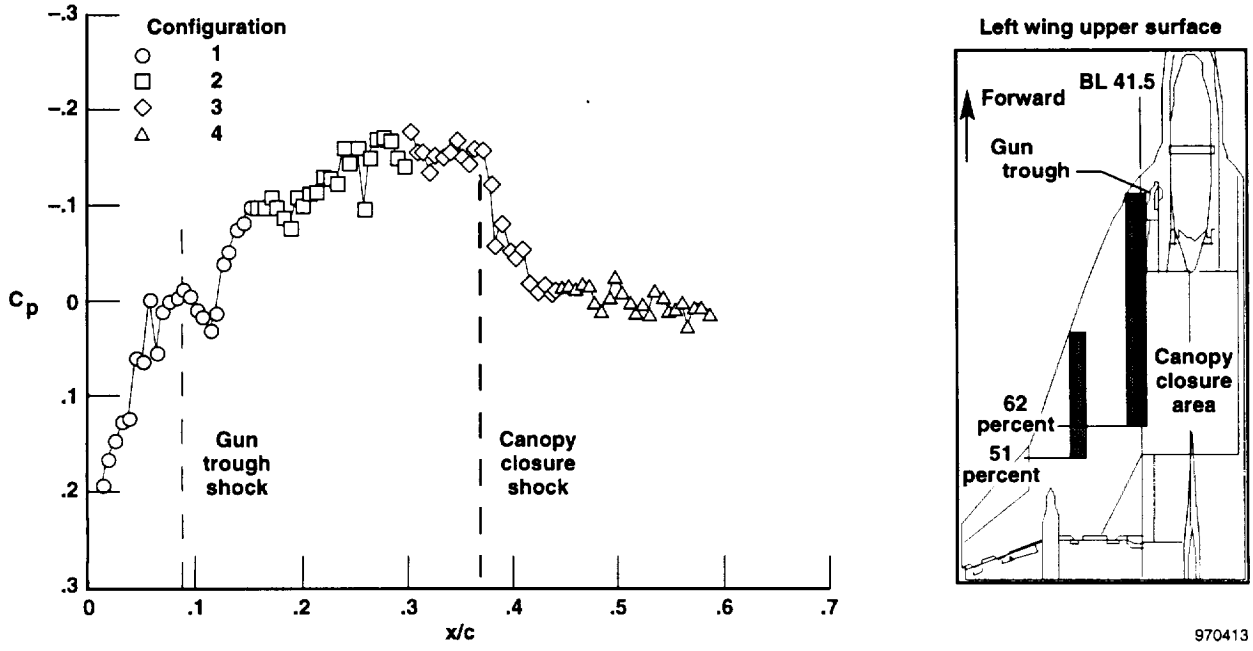

(a) Upper inboard pressure belt, group A.

Figure 10. Composite plot of upper surface pressures with gun trough cover at Mach 1.7, an altitude of 50,000 ft, and an angle of attack of 3.3°.

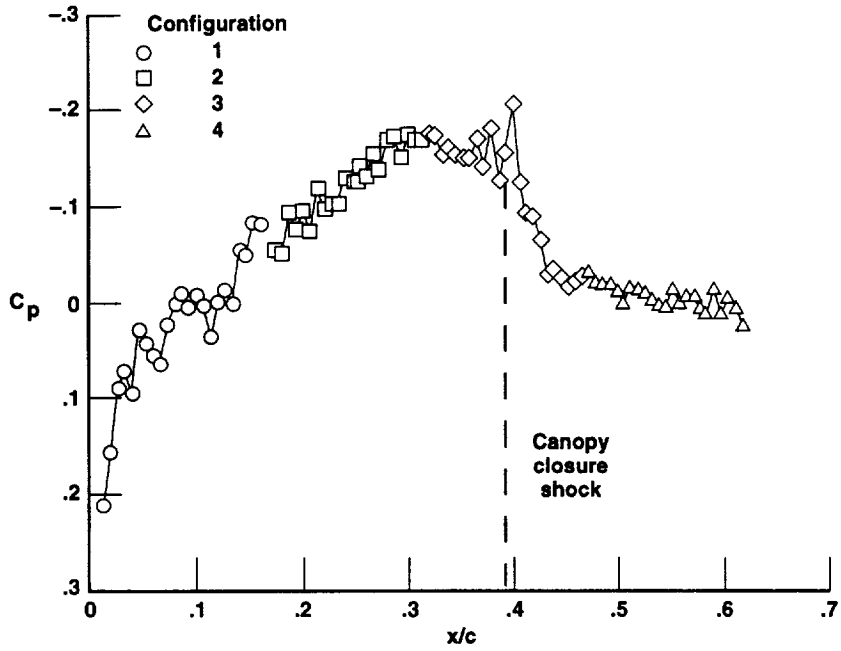

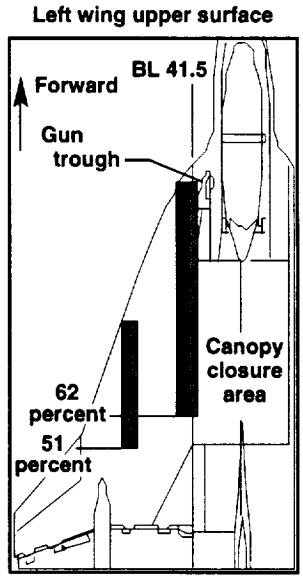

(b) Upper inboard pressure belt, group C.

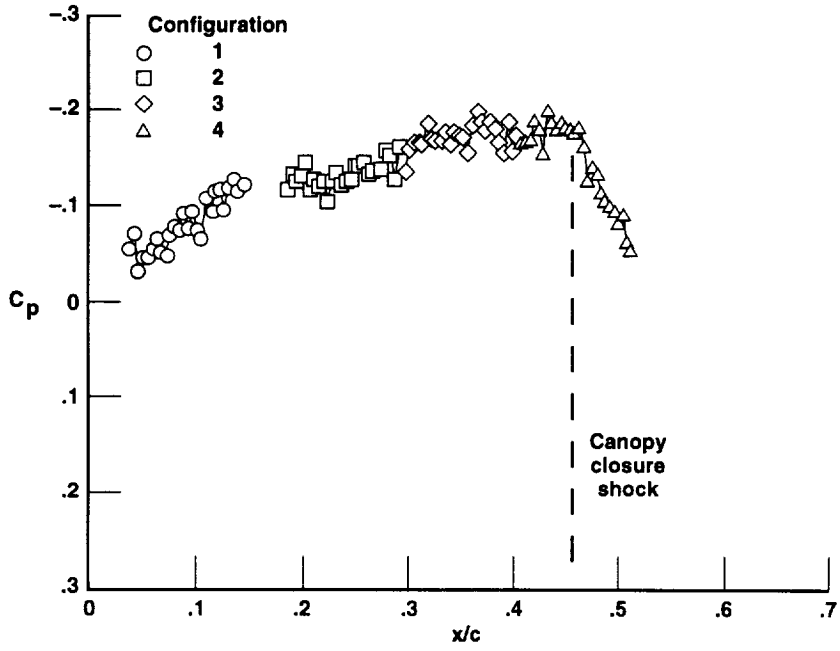

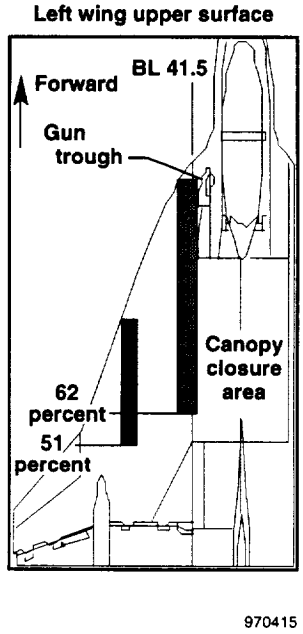

(c) Upper outboard pressure belt.

Figure 10. Concluded.

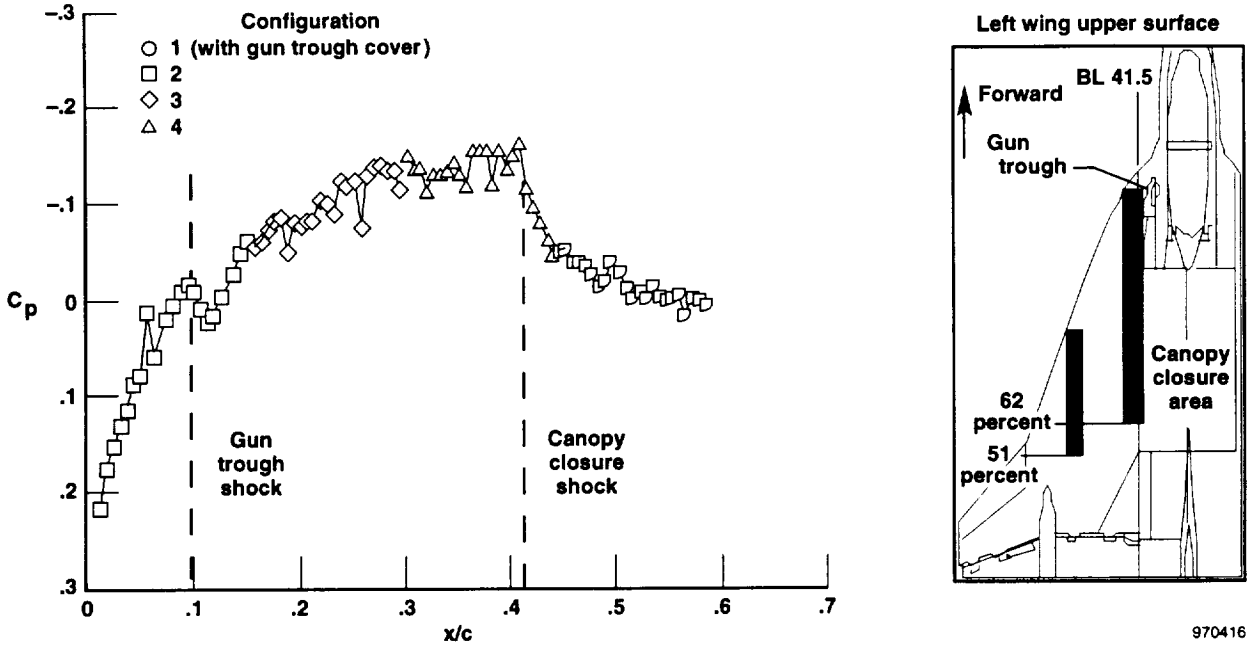

(a) Upper inboard pressure belt, group A.

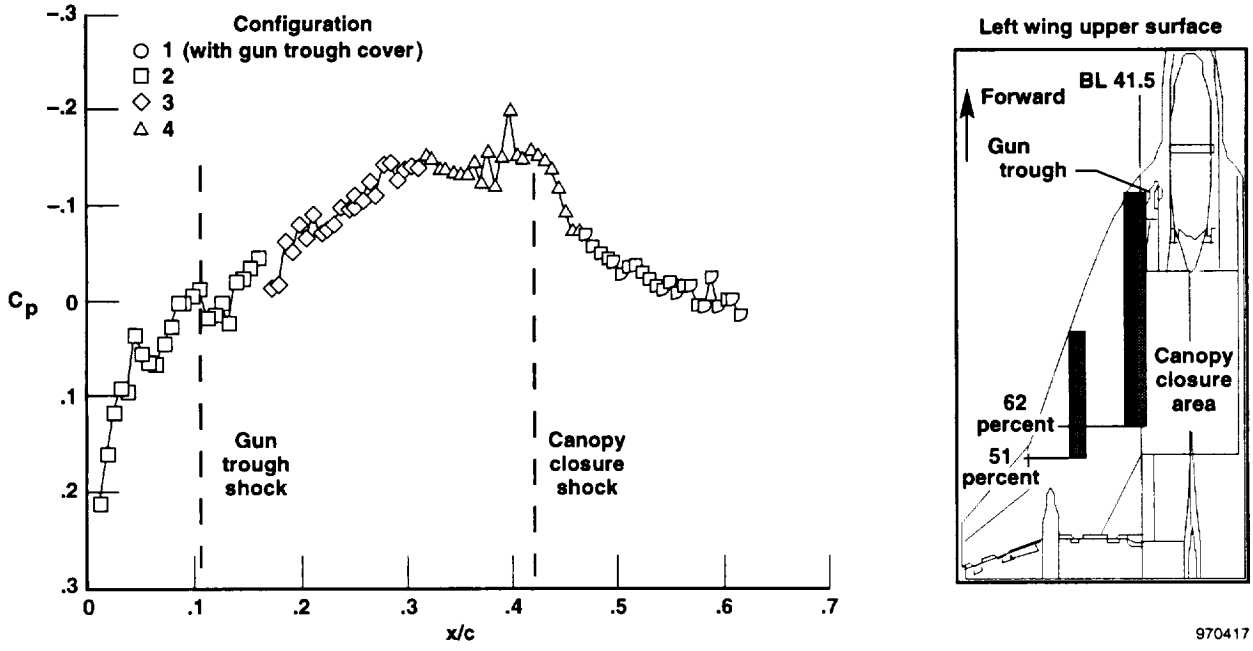

(b) Upper inboard pressure belt, group C.

Figure 11. Composite plot of upper surface pressures, Mach 1.9, an altitude of 50,000 ft, and an angle of attack of 3.4°.

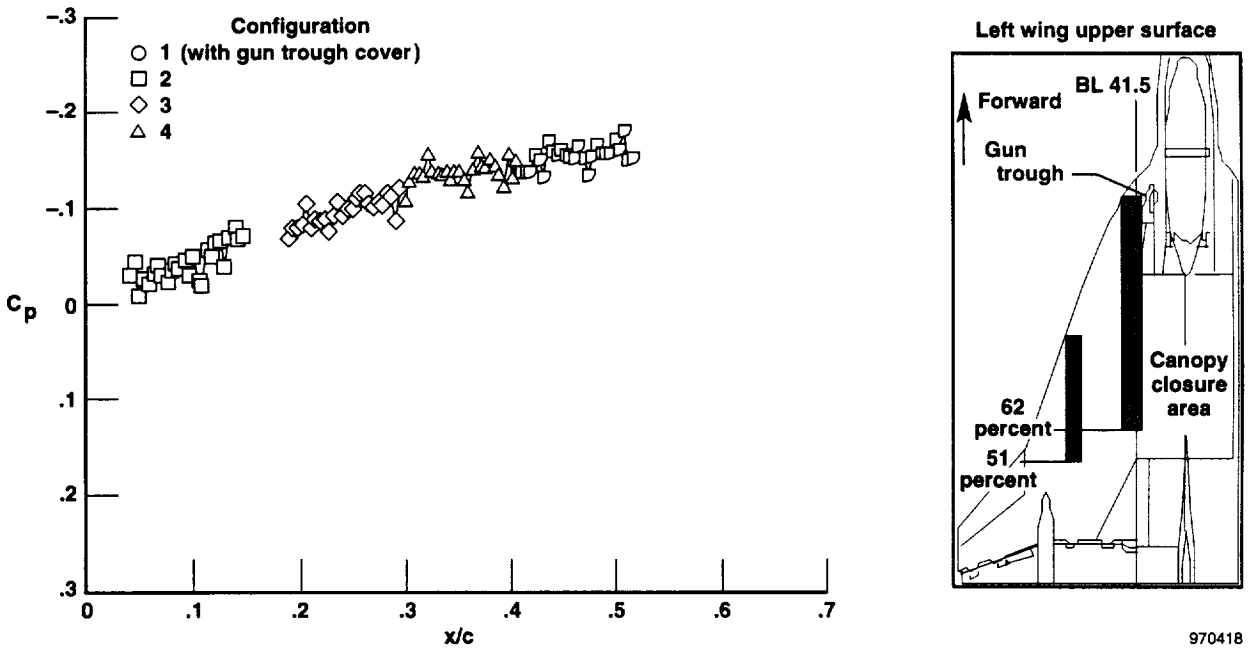

(c) Upper outboard pressure belt.

Figure 11. Concluded.

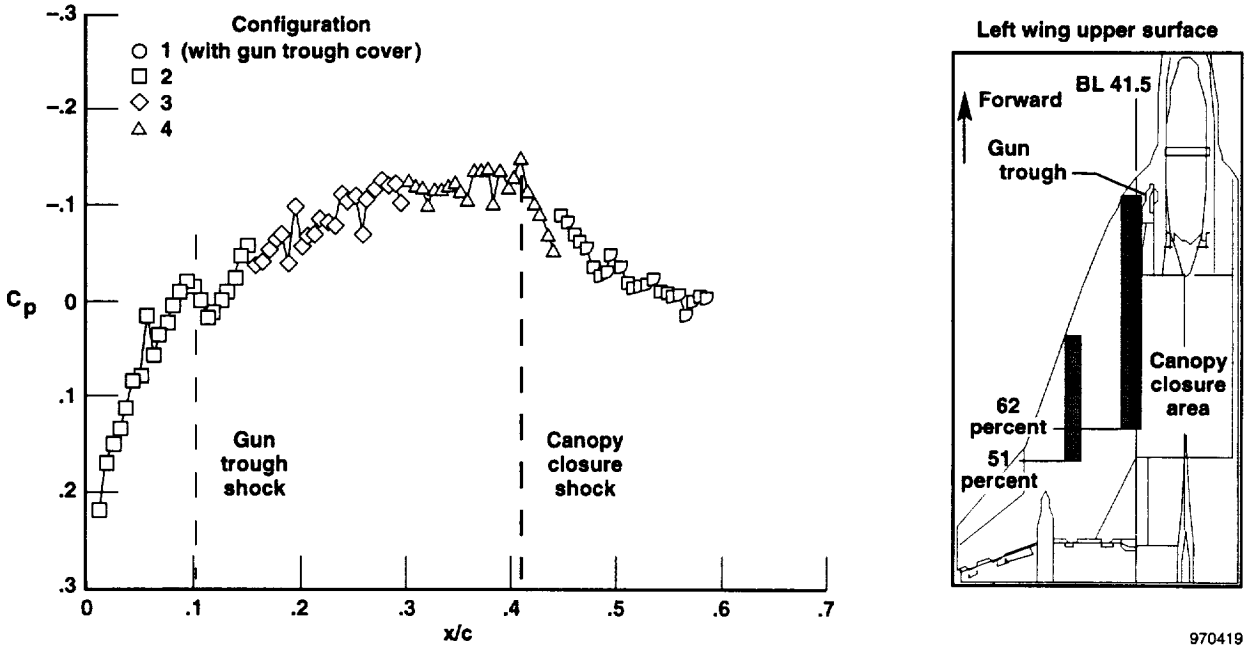

(a) Upper inboard pressure belt, group A.

Figure 12. Composite plot of pressures at Mach 2.0, an altitude of 50,000 ft, and an angle of attack of 3.5°.

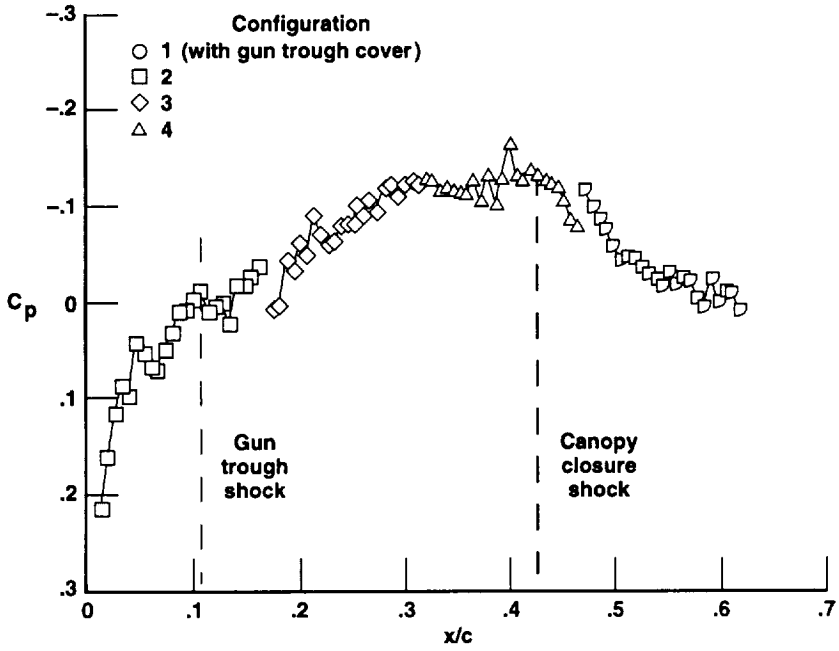

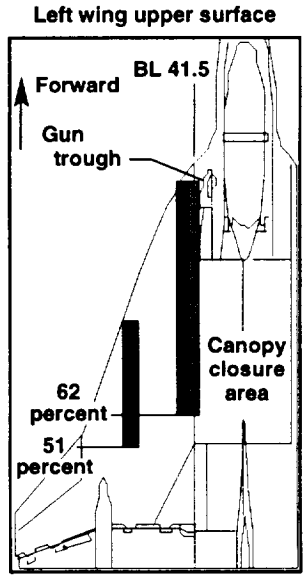

(b) Upper inboard pressure belt, group C.

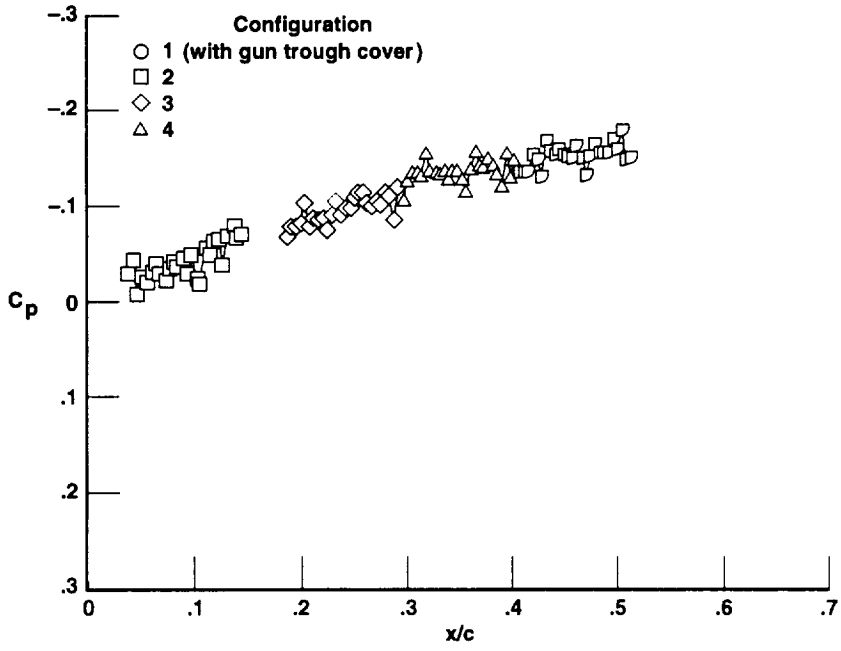

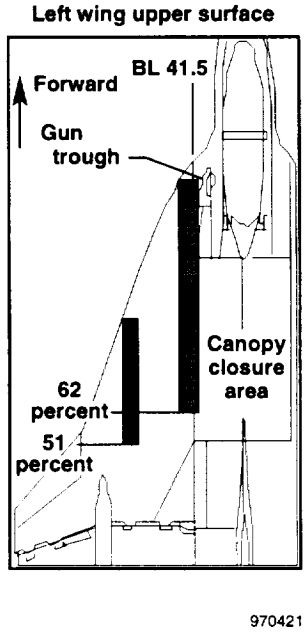

(c) Upper outboard pressure belt.

Figure 12. Concluded.

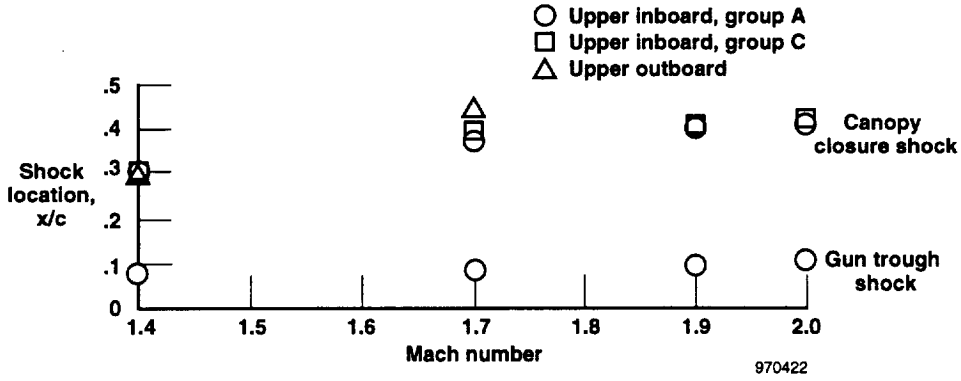

(a) Shock wave locations.

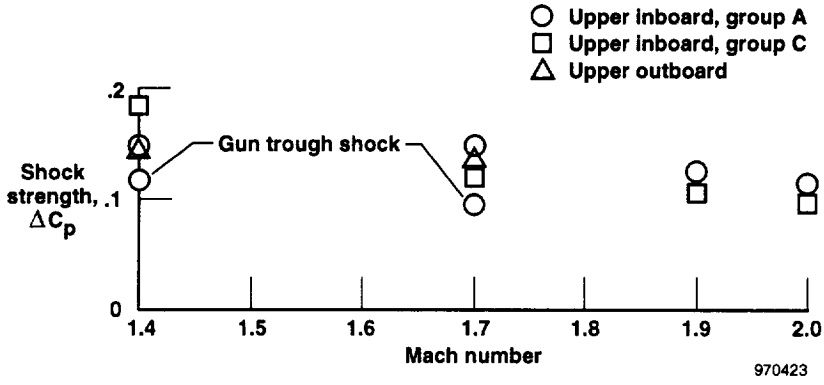

(b) Shock wave strength.

Figure 13. Position and strength of shock waves generated by the gun trough and canopy closure for different pressure belts. The shock strength of outboard at Mach 1.7 is unverified. The shock extends beyond the last pressure orifice.

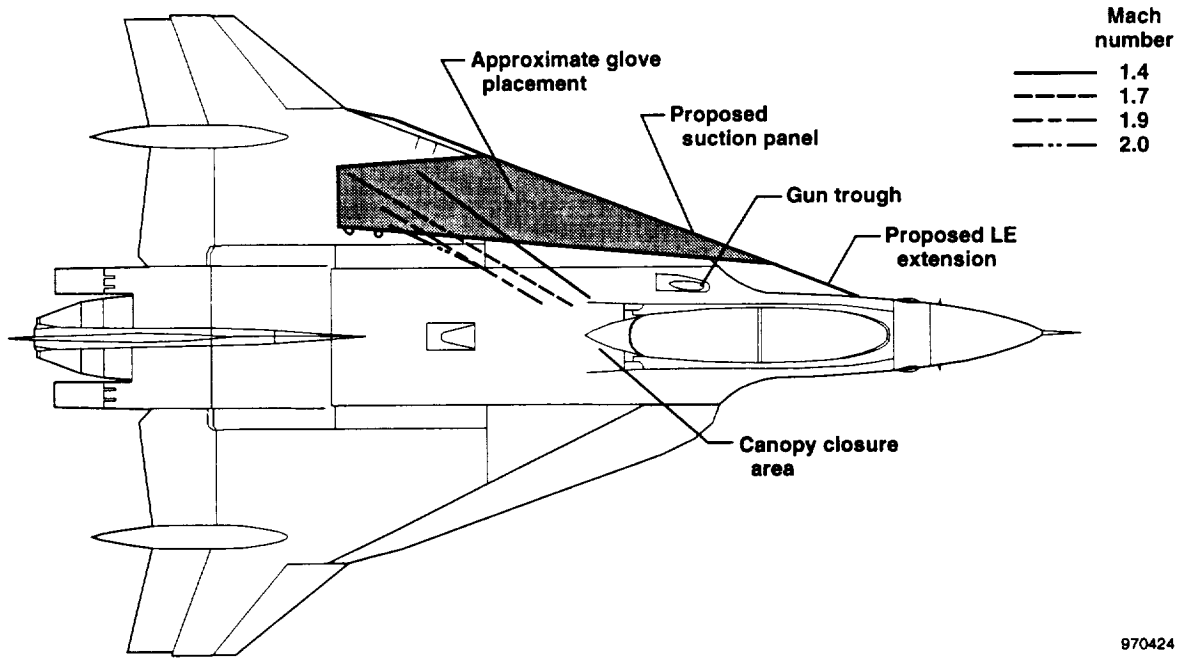

Figure 14. Upper planform of the F-16XL ship 2 with the SLFC glove. Shock waves from the canopy closure area are shown for various Mach numbers.

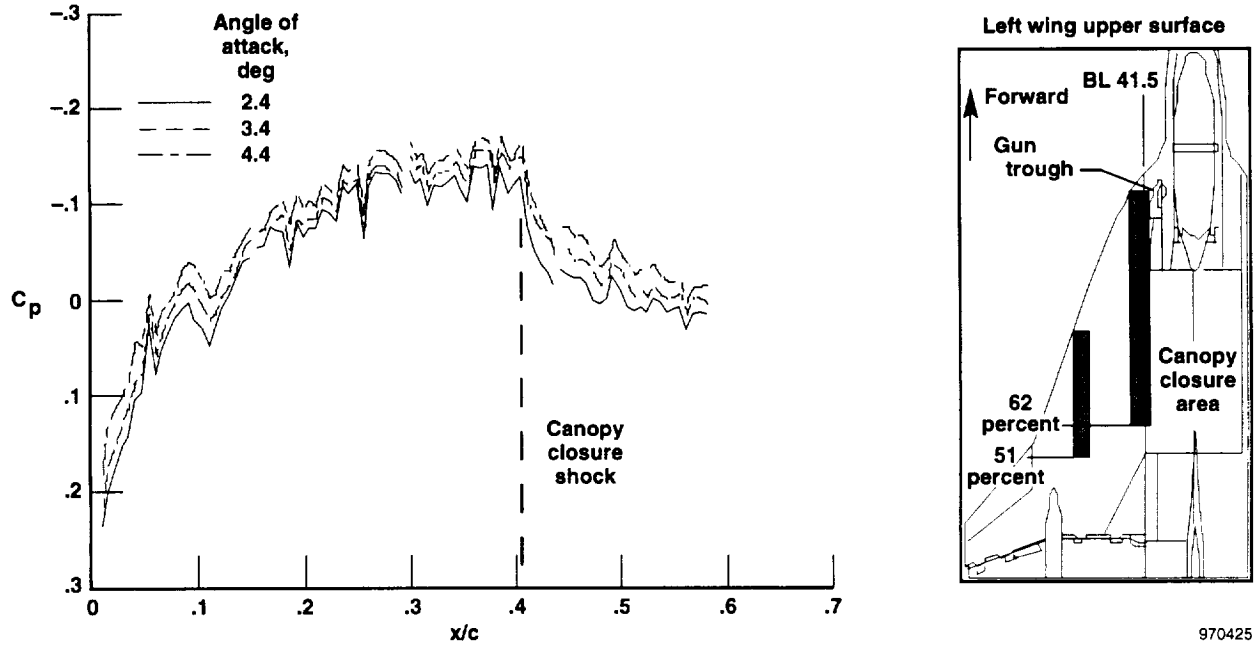

Figure 15. Influence of Angle-of-attack on the upper surface pressure distributions at Mach 1.9 and an altitude of 50,000 ft, group A.

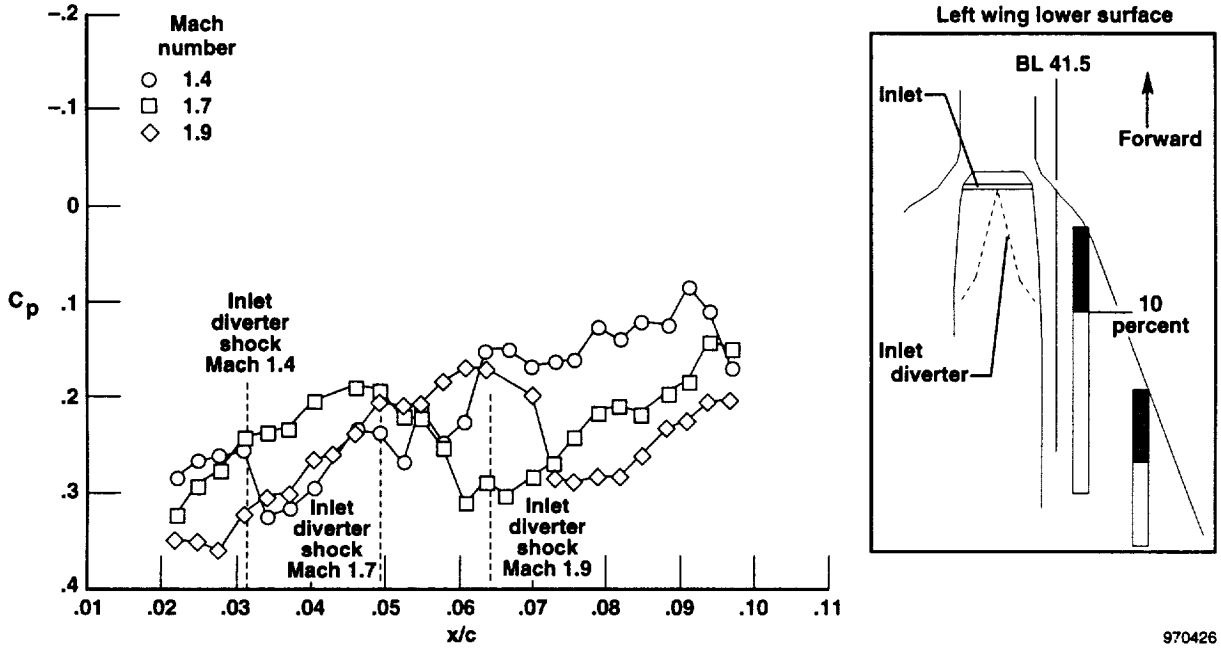

Figure 16. Lower surface pressure distributions of baseline aircraft at an indicated angle of attack of 2.0°.

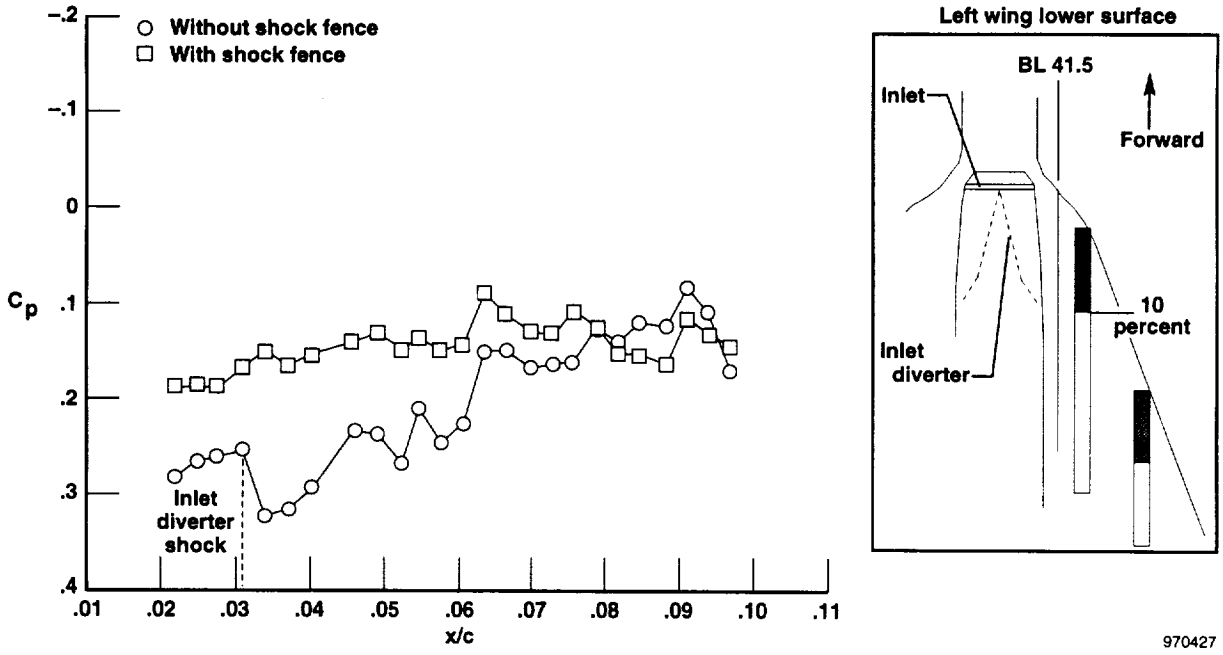

Figure 17. Lower surface inboard pressure distribution at Mach 1.4, an altitude of 50,000 ft, and an angle of attack of 3.2°.

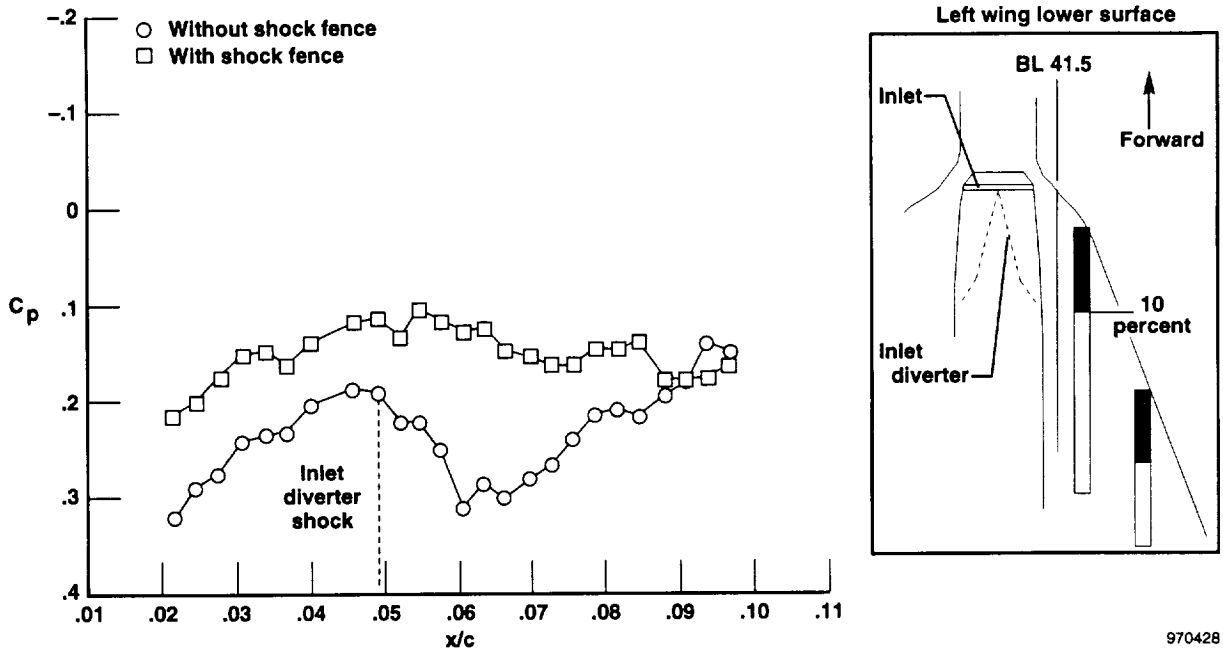

Figure 18. Lower inboard pressure belt at Mach 1.7, an altitude of 50,000 ft, and an angle of attack of 3.3°.

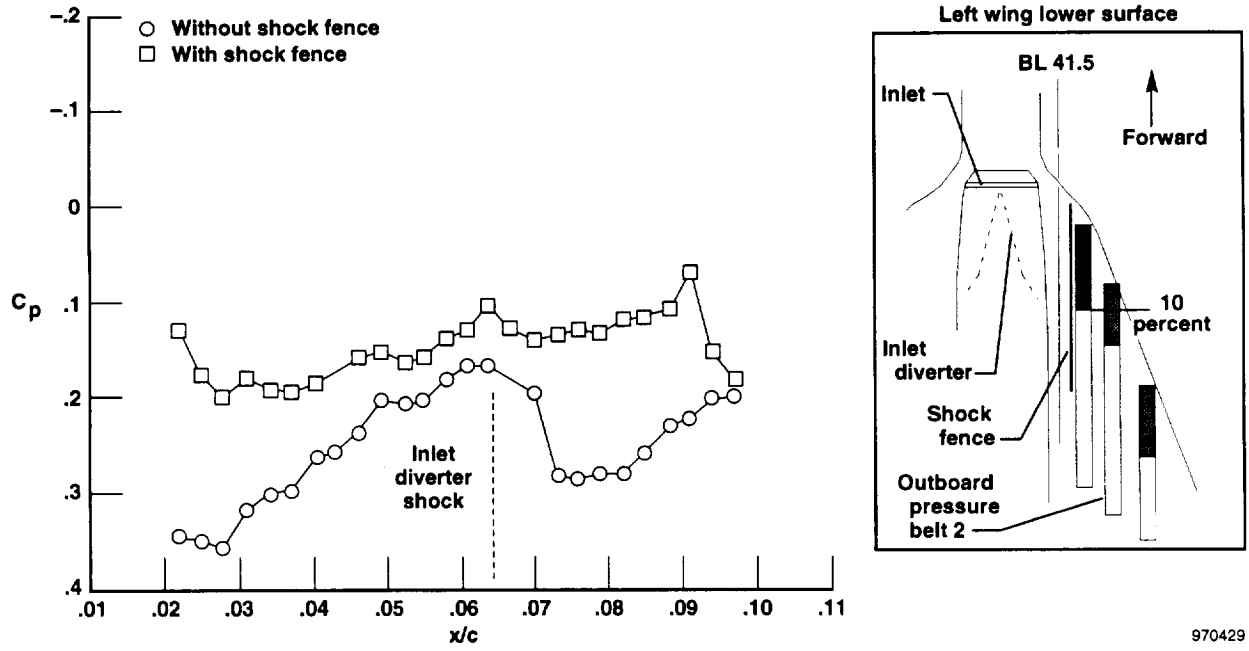

(a) Lower inboard pressure belt.

Figure 19. Lower surface pressure distributions for Mach 1.9, an altitude of 50,000 ft, and an angle of attack of 3.4°.

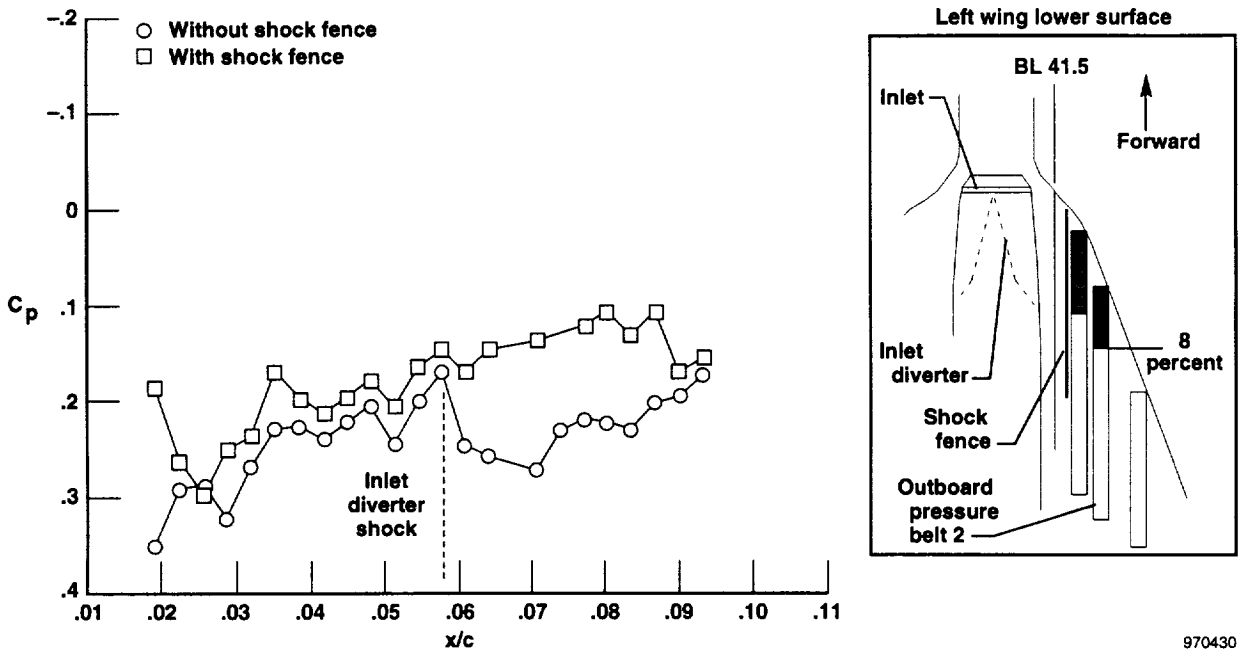

(b) Lower outboard pressure belt 2.

Figure 19. Concluded.

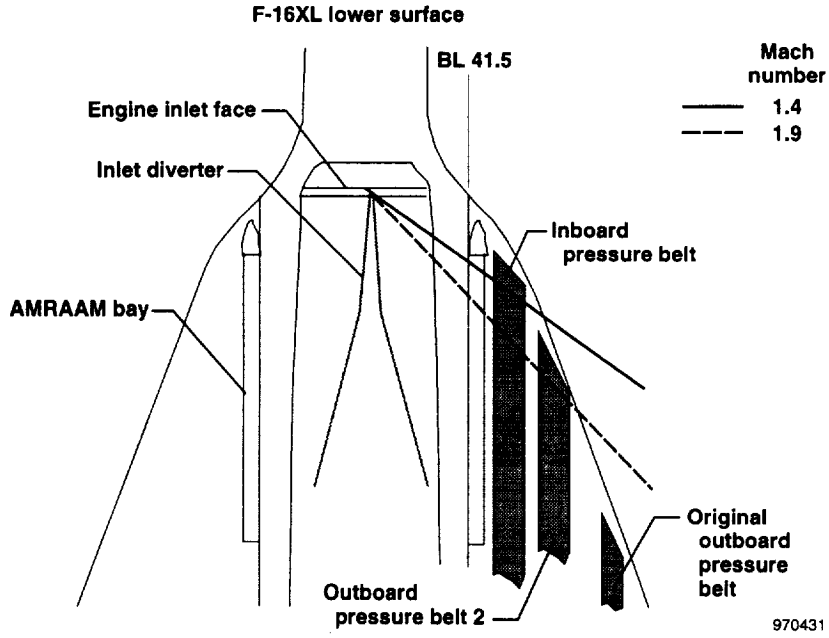

Figure 20. F-16XL lower surface shock waves with no shock fence installed.

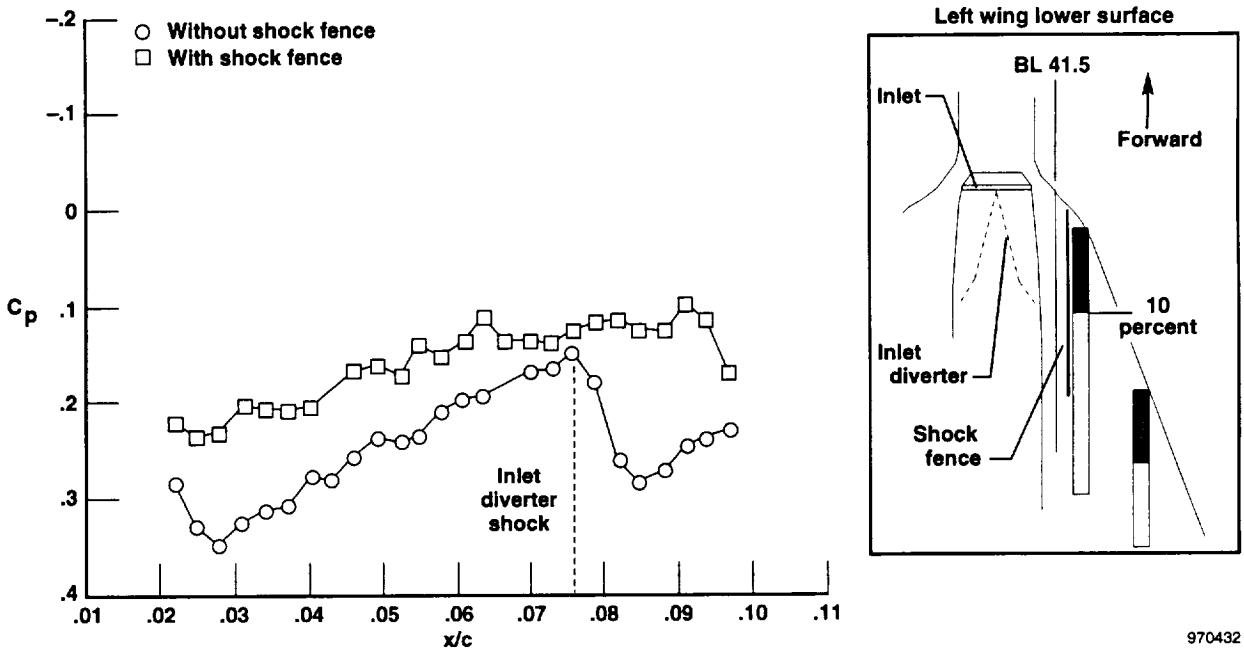

(a) Lower inboard pressure belt.

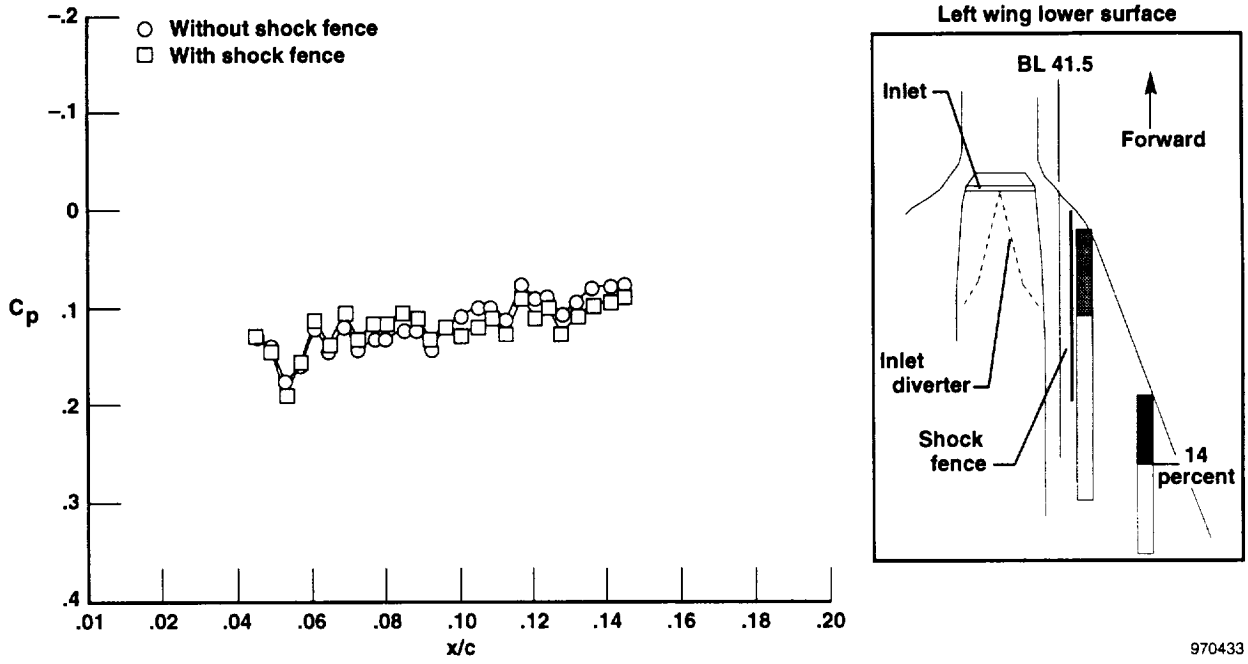

(b) Lower outboard pressure belt.

Figure 21. Lower surface pressure distributions at Mach 2.0, an altitude of 50,000 ft, and an angle of attack of 3.5°.

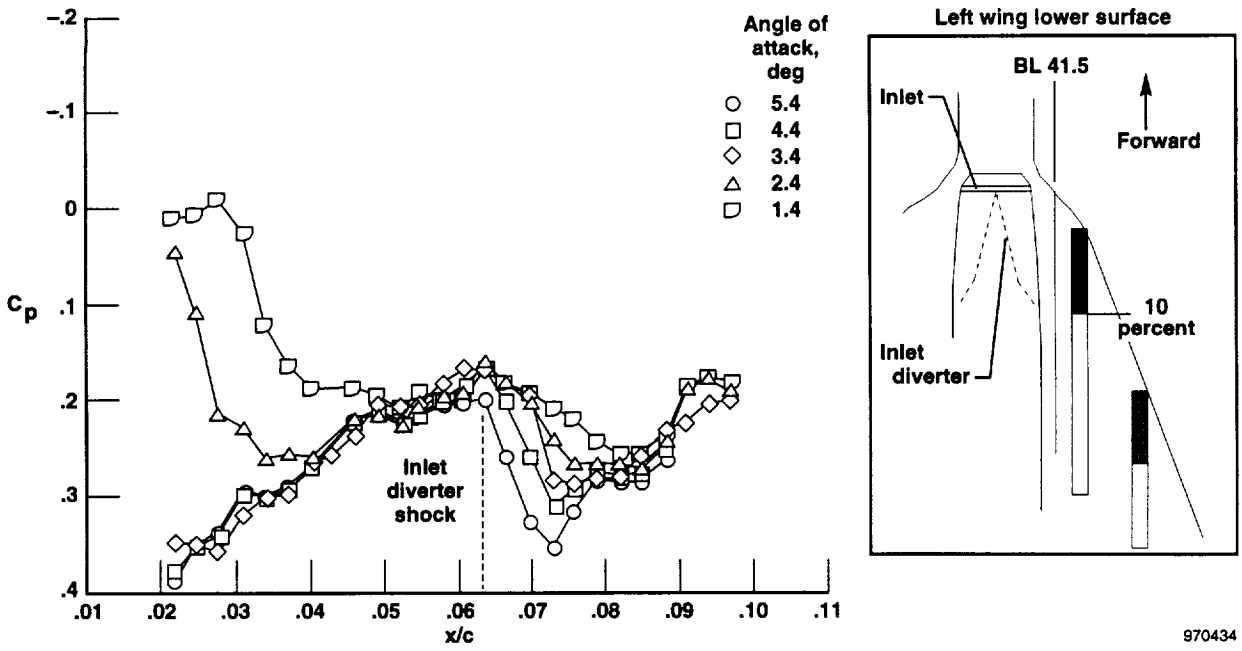

(a) Lower inboard pressure belt without the shock fence.

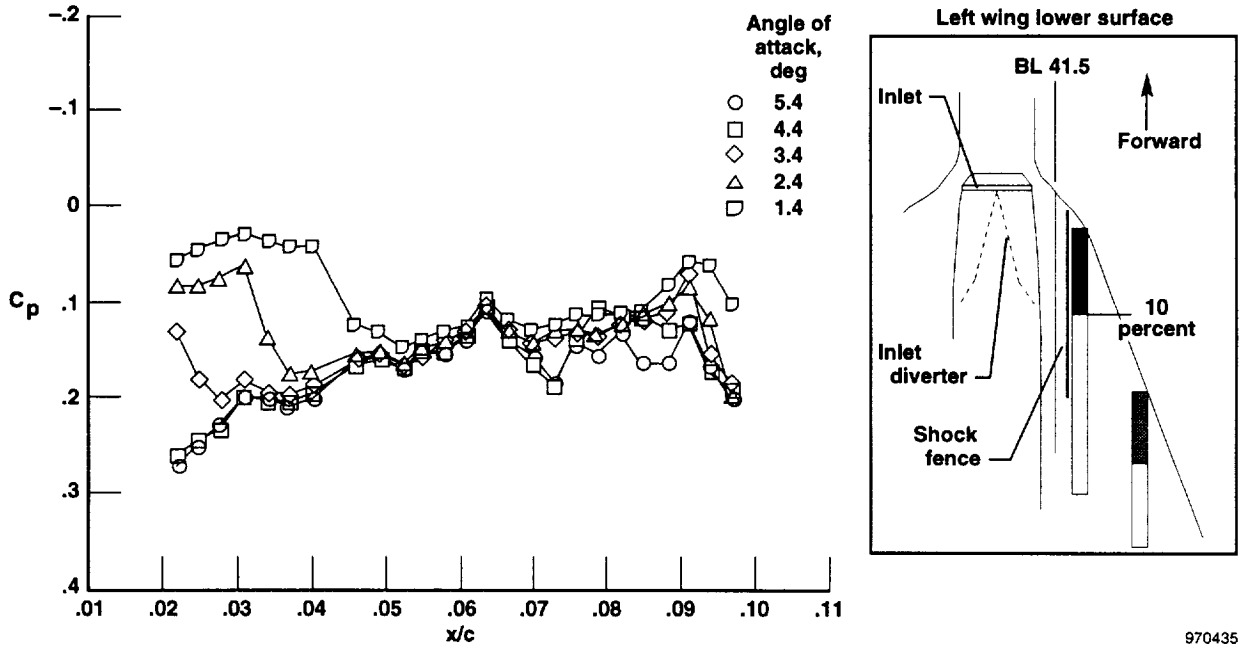

(b) Lower inboard pressure belt with the shock fence.

Figure 22. Influence of angle of attack on pressure distributions at Mach 1.9 and an altitude of 50,000 ft.

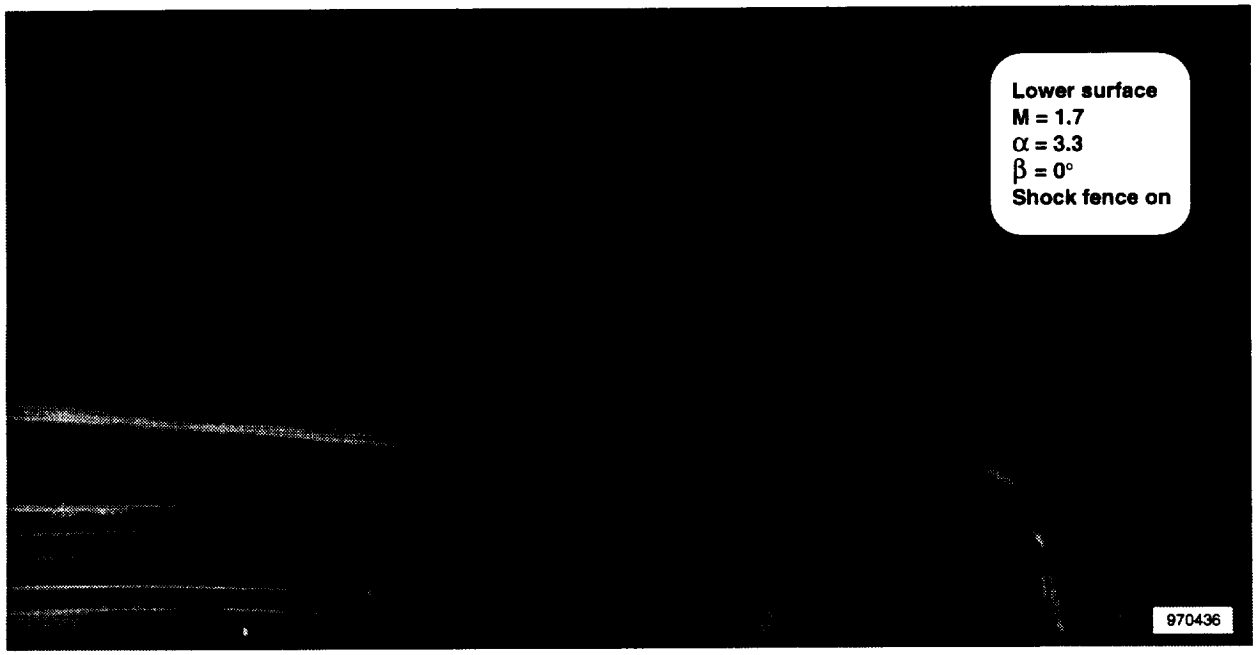

(a) Mach 1.7 and an angle of attack of 3.3°.

(b) Mach 1.9 and an angle of attack of 3.3°.

Figure 23. Lower surface oil flow patterns (shock fence off) during tests in the NASA Langley Research Center Unitary Plan Supersonic Wind Tunnel.

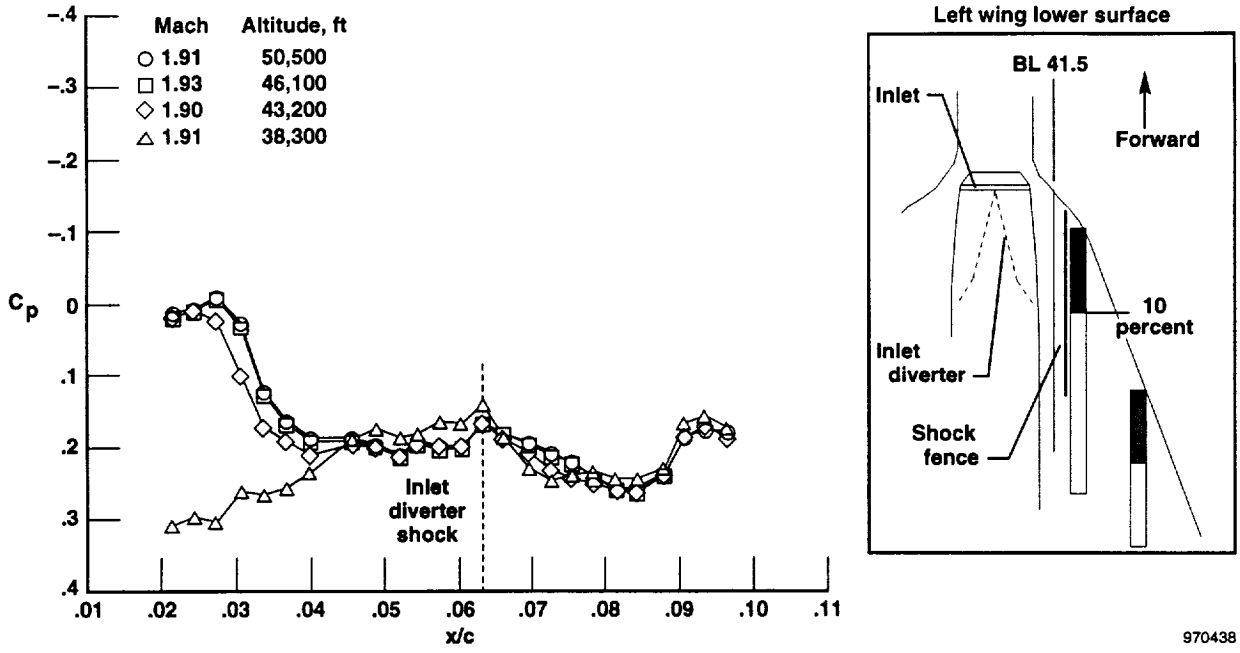

(a) Angle of attack of 1.4°.

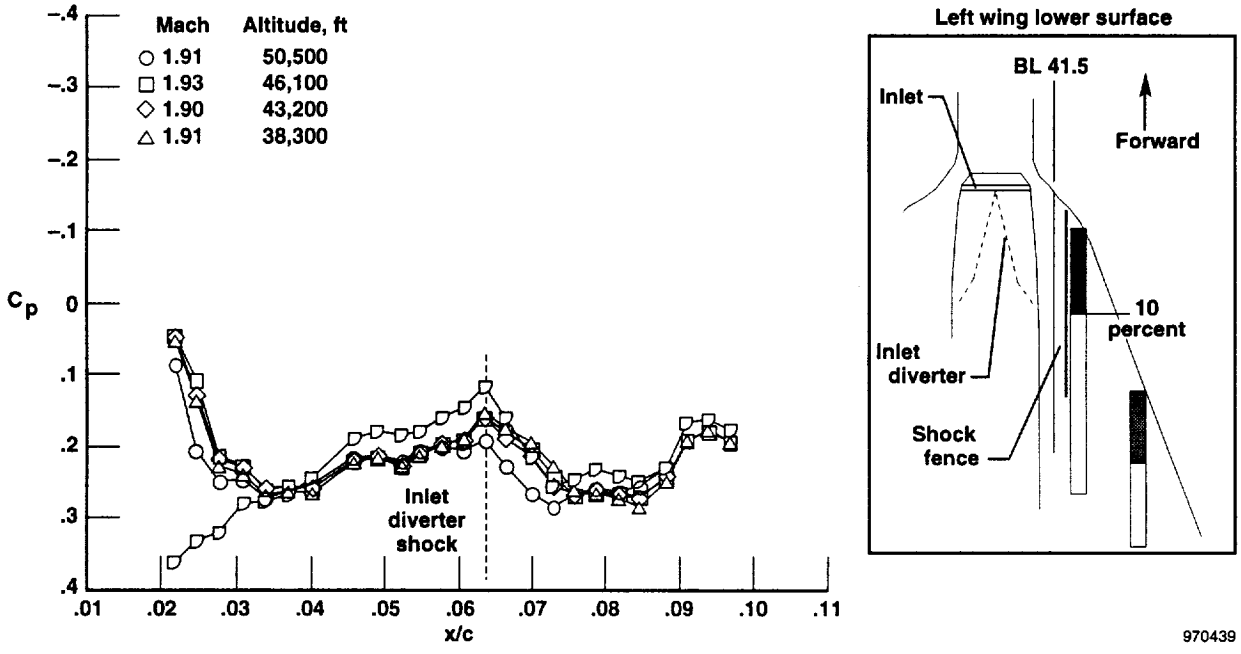

(b) Angle of attack of 2.4°.

Figure 24. Influence of altitude (inlet mass flow) and angle of attack at Mach 1.9 on lower surface inboard pressures.

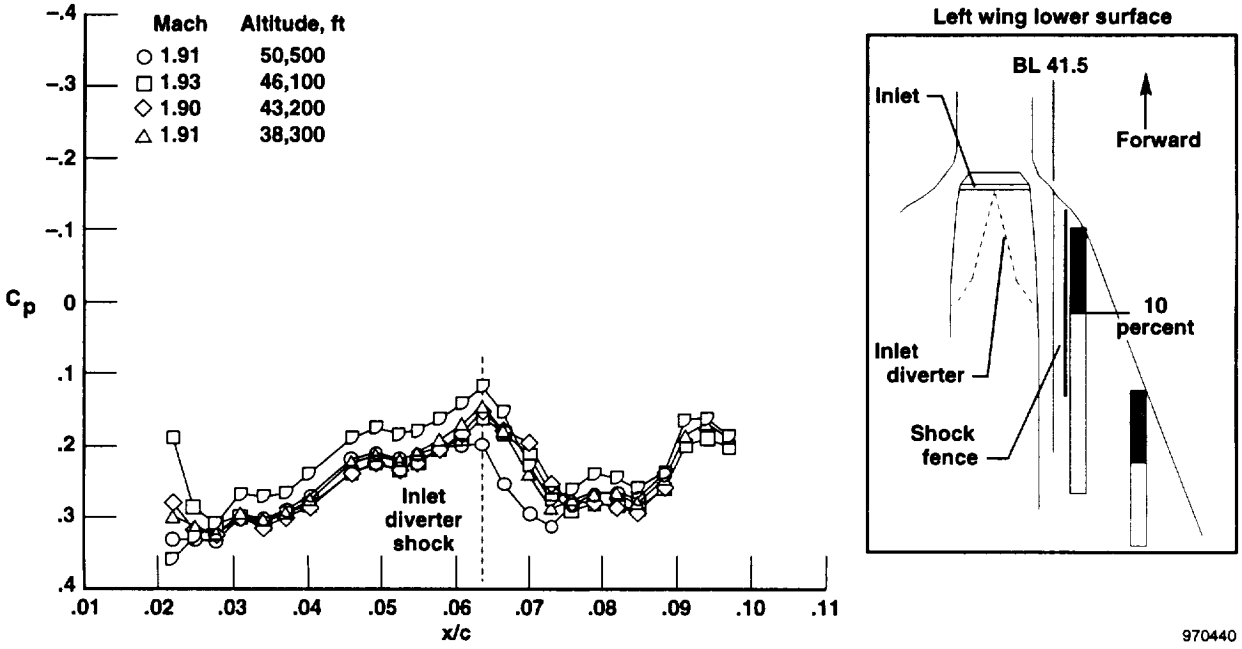

(c) Angle of attack of 3.4°.

Figure 24. Concluded.

REPORT DOCUMENTATION PAGE

Form Approved
OMB No. 0704-0188

1. AGENCY USE ONLY (Leave blank)	2. REPORT DATE	3. REPORT TYPE AND DATES COVERED
	October 1997	Technical Memorandum

4. TITLE AND SUBTITLE

F-16XL Wing Pressure Distributions and Shock Fence Results from Mach 1.4 to Mach 2.0

5. FUNDING NUMBERS

529 31 24 00 24 00

6. AUTHOR(S)

Stephen F. Landers, John A. Saltzman, and Lisa J. Bjarke

7. PERFORMING ORGANIZATION NAME(S) AND ADDRESS(ES)

NASA Dryden Flight Research Center
P.O. Box 273
Edwards, California 93523-0273

8. PERFORMING ORGANIZATION REPORT NUMBER

H-2055

9. SPONSORING/MONITORING AGENCY NAME(S) AND ADDRESS(ES)

National Aeronautics and Space Administration
Washington, DC 20546-0001

10. SPONSORING/MONITORING AGENCY REPORT NUMBER

NASA/TM-97-206219

11. SUPPLEMENTARY NOTES

Stephen F. Landers and John A. Saltzman, PRC Inc., Edwards, California.
Lisa J. Bjarke, NASA Dryden Flight Research Center, Edwards, California.

12a. DISTRIBUTION/AVAILABILITY STATEMENT

Unclassified—Unlimited
Subject Category 02

12b. DISTRIBUTION CODE

13. ABSTRACT (Maximum 200 words)

Chordwise pressure distributions were obtained in-flight on the upper and lower surfaces of the F-16XL ship 2 aircraft wing between Mach 1.4 and Mach 2.0. This experiment was conducted to determine the location of shock waves which could compromise or invalidate a follow-on test of a large chord laminar flow control suction panel. On the upper surface, the canopy closure shock crossed an area which would be covered by a proposed laminar flow suction panel. At the laminar flow experiment design Mach number of 1.9, 91 percent of the suction panel area would be forward of the shock. At Mach 1.4, that value reduces to 65 percent. On the lower surface, a shock from the inlet diverter would impinge on the proposed suction panel leading edge. A chordwise plate mounted vertically to deflect shock waves, called a shock fence, was installed between the inlet diverter and the leading edge. This plate was effective in reducing the pressure gradients caused by the inlet shock system.

14. SUBJECT TERMS	15. NUMBER OF PAGES
F-16XL aircraft, Supersonic transports, Shockwaves, Pressure distribution, Laminar flow	44
	16. PRICE CODE AO3

17. SECURITY CLASSIFICATION OF REPORT	18. SECURITY CLASSIFICATION OF THIS PAGE	19. SECURITY CLASSIFICATION OF ABSTRACT	20. LIMITATION OF ABSTRACT
Unclassified	Unclassified	Unclassified	Unlimited

NSN 7540-01-280-5500 *Available from the NASA Center for AeroSpace Information, 800 Elkridge Landing Road, Linthicum Heights, MD 21090; (301)621-0390*

Standard Form 298 (Rev. 2-89)
Prescribed by ANSI Std. Z39-18
298-102